Cell Stem Cell
Article

Modeling a Genetic Risk for Schizophrenia in iPSCs and Mice Reveals Neural Stem Cell Deficits Associated with Adherens Junctions and Polarity

Ki-Jun Yoon,[1,2] Ha Nam Nguyen,[1,3] Gianluca Ursini,[4] Fengyu Zhang,[4] Nam-Shik Kim,[1,2] Zhexing Wen,[1,2] Georgia Makri,[1,2] David Nauen,[5] Joo Heon Shin,[4] Youngbin Park,[1] Raeeun Chung,[1] Eva Pekle,[1] Ce Zhang,[1,2] Maxwell Towe,[1] Syed Mohammed Qasim Hussaini,[1] Yohan Lee,[6] Dan Rujescu,[7] David St. Clair,[8] Joel E. Kleinman,[4] Thomas M. Hyde,[4] Gregory Krauss,[2] Kimberly M. Christian,[1,2] Judith L. Rapoport,[6] Daniel R. Weinberger,[2,4,9] Hongjun Song,[1,2,3,9,*] and Guo-li Ming[1,2,3,9,*]
[1]Institute for Cell Engineering
[2]Department of Neurology
[3]Graduate Program in Cellular and Molecular Medicine
[4]Lieber Institute for Brain Development
[5]Department of Pathology
Johns Hopkins University School of Medicine, Baltimore, MD 21205, USA
[6]Child Psychiatry Branch, National Institute of Mental Health, Bethesda, MD 20892, USA
[7]Department of Psychiatry, Ludwig-Maximilians University, Nussbaumstrasse 7, 80336, Munich, Germany
[8]University of Aberdeen Royal Cornhill Hospital, Aberdeen AB25 2ZD, UK
[9]The Solomon H. Snyder Department of Neuroscience, Johns Hopkins University School of Medicine, Baltimore, MD 21205, USA
*Correspondence: gming1@jhmi.edu (G.-l.M.), shongju1@jhmi.edu (H.S.)
http://dx.doi.org/10.1016/j.stem.2014.05.003

SUMMARY

Defects in brain development are believed to contribute toward the onset of neuropsychiatric disorders, but identifying specific underlying mechanisms has proven difficult. Here, we took a multifaceted approach to investigate why 15q11.2 copy number variants are prominent risk factors for schizophrenia and autism. First, we show that human iPSC-derived neural progenitors carrying 15q11.2 microdeletion exhibit deficits in adherens junctions and apical polarity. This results from haploinsufficiency of *CYFIP1*, a gene within 15q11.2 that encodes a subunit of the WAVE complex, which regulates cytoskeletal dynamics. In developing mouse cortex, deficiency in CYFIP1 and WAVE signaling similarly affects radial glial cells, leading to their ectopic localization outside of the ventricular zone. Finally, targeted human genetic association analyses revealed an epistatic interaction between CYFIP1 and WAVE signaling mediator ACTR2 and risk for schizophrenia. Our findings provide insight into how CYFIP1 regulates neural stem cell function and may contribute to the susceptibility of neuropsychiatric disorders.

INTRODUCTION

Neuropsychiatric disorders, including schizophrenia and autism, are debilitating conditions that are postulated to have a neurodevelopmental etiology (Geschwind, 2009; Weinberger, 1987). Significant progress has been made to identify the genetic basis of these disorders. In addition to single-nucleotide polymorphisms (SNPs), submicroscopic variations in DNA copy number (CNVs) are also widespread in human genomes and specific CNVs have been identified as significant risk factors for schizophrenia and autism (Malhotra and Sebat, 2012). Because CNVs frequently contain multiple genes and are more difficult to model in mice using traditional gene targeting techniques, we know little about how these CNVs affect neural development. Novel approaches are needed to investigate these genetic risk factors in neural development and identify their signaling mechanisms, which in turn could generate new hypotheses for identification of additional risk factors.

15q11.2 CNVs have emerged as prominent risk factors for various neuropsychiatric disorders, including schizophrenia, autistic spectrum disorder, and intellectual disability (Malhotra and Sebat, 2012). 15q11.2 microdeletion (15q11.2 del) was identified as one of the most frequent CNVs associated with increased risk for schizophrenia in two large studies (International Schizophrenia Consortium, 2008; Stefansson et al., 2008), a finding subsequently confirmed in additional cohorts (Kirov et al., 2009; Tam et al., 2010; Zhao et al., 2013a). Even in normal subjects, 15q11.2 del is associated with cognitive variation and changes in structural measures on MRI scanning (Stefansson et al., 2014). 15q11.2 CNVs encompass four genes, *nonimprinted in Prader/Willi Angelman 1* and *2* (*NIPA1* and *NIPA2*), *CYFIP1*, and *TUBGCP5* (Figure 1A). While little is known about functions of these genes in mammalian neural development, CYFIP1 has been shown to interact with Rac1 (Kobayashi et al., 1998), FMRP (Schenck et al., 2001), and eIF4E (Napoli et al., 2008). Biochemical studies have also identified CYFIP1 as a regulator of the WAVE complex, consisting of WAVE1, WAVE2, Nap1, and Abi1, a complex known to regulate Arp2/3-mediated actin polymerization and membrane protrusion formation in nonneuronal cell lines (Kobayashi et al., 1998; Kunda et al., 2003; Steffen et al., 2004). The function of WAVE signaling in mammalian neurogenesis is not well understood.

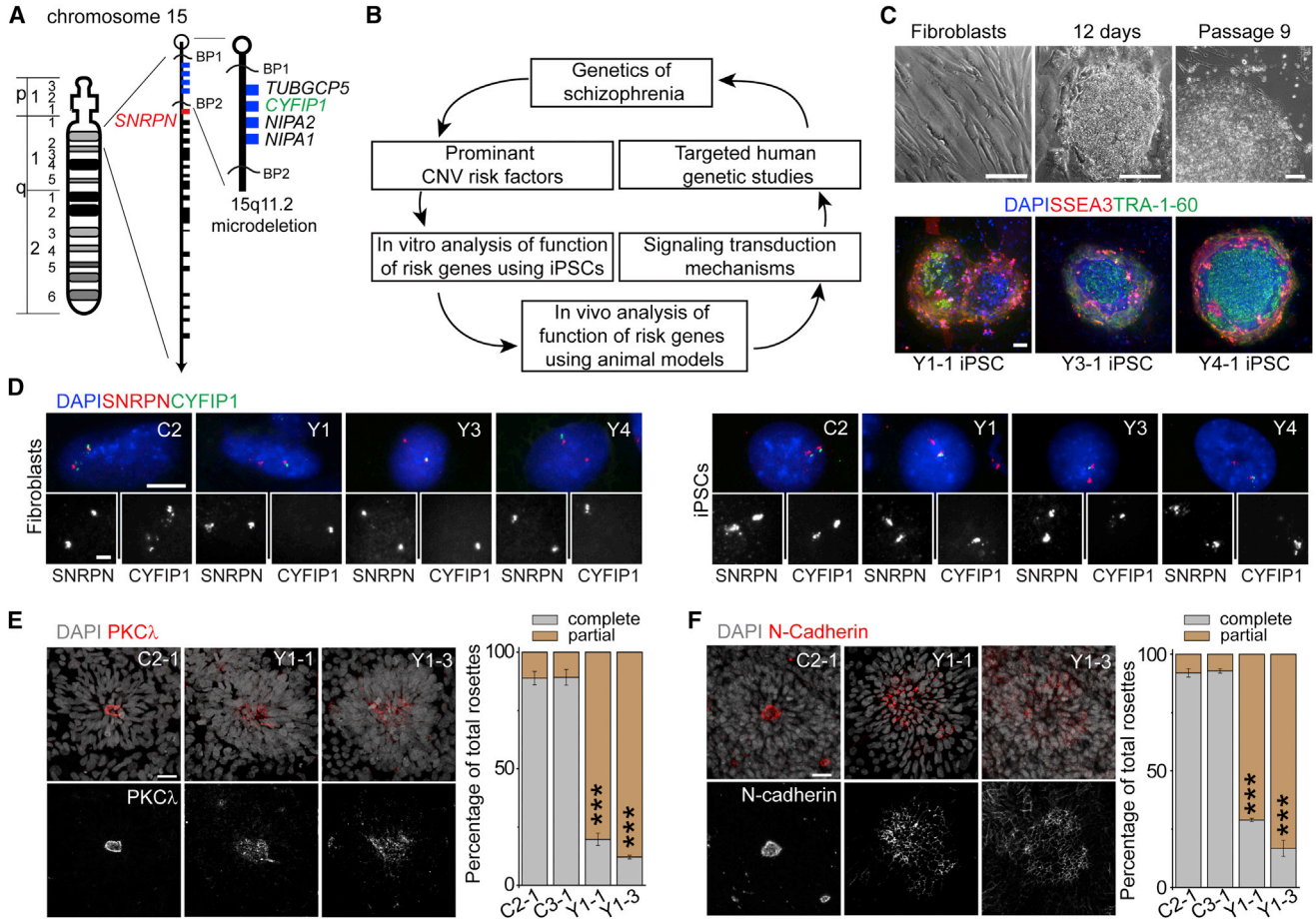

Figure 1. iPSC Derivation and Aberrant Neural Rosette Formation of hNPCs Differentiated from iPSC Lines Carrying 15q11.2 Del

(A) An ideogram of Chromosome 15 with proximal 15q11.2 region expanded. Blue boxes indicate the four deleted genes within 15q11.2 del, including *CYFIP1*.

(B) A schematic summary of the current study design.

(C) Sample light microscopic images and fluorescent images of fibroblasts and iPSC colonies for immunostaining of pluripotency markers. Scale bars represent 100 μm.

(D) Sample fluorescence in situ hybridization (FISH) images of donor fibroblasts and derived iPSC lines. Two FISH probes, one for *CYFIP1* locus and one for *SNRPN* locus (outside of 15q11.2; see A for the genomic location), were used. Scale bar represents 10 μm (upper panels) and 2 μm (lower panels).

(E and F) Defects in adherens junctions and apical polarity of hNPCs derived from iPSCs with 15q11.2 del. Shown on the left are sample confocal images of immunostaining of atypical PKCλ (E) and N-cadherin (F) for neural rosettes differentiated from iPSCs by the monolayer method. Scale bars represent 20 μm. Shown on the right are quantifications of neural rosettes with complete "apical ring-like structure" (≥90% coverage of apical-ring circumference with atypical PKCλ or N-cadherin immunoreactivity) or "partial/scattered" (<90% coverage). Values represent mean ± SEM (n = 3 cultures; ***$p < 0.001$; Student's t test). See also Figures S1 and S2 and Tables S1 and S2.

Patient-derived induced pluripotent stem cells (iPSCs) provide a new means to investigate how risk factors affect nervous system development (Bellin et al., 2012; Christian et al., 2012). Reprogrammed from somatic cells, iPSCs capture identical risk alleles as the donor individual and provide a renewable resource of previously inaccessible, disease-relevant human cell types to facilitate molecular and cellular investigations. In this emerging new field, recent iPSC studies were mostly "proof-of-principle" experiments that confirmed previous findings from animal and postmortem human studies; its promise as a discovery tool is just beginning to be realized.

While 15q11.2 del is linked to schizophrenia, common variants within the deletion region have not shown similar association in case control studies, possibly because of the weak impact of common SNPs on biological functions of individual genes. To mimic the large dose effect of a whole gene deletion, we hypothesized that genetic interactions within the biological network linked to the function of specific genes within 15q11.2 del would rise to the level of clinical association and that patient-derived iPSC studies could provide an entry point to identify these networks (Figure 1B). We established iPSC lines from three individuals carrying 15q11.2 del and compared them with iPSCs from five individuals without the CNV. Analysis of iPSC-derived neural rosettes with 15q11.2 del revealed impairments in adherens junctions and polarity of human neural progenitor cells (hNPCs) due to WAVE complex destabilization. Pinpointing *CYFIP1*-haploinsufficiency within 15q11.2 as a underlying cause of hNPC defects then guided our investigation of CYFIP1 and its signaling

via the WAVE complex in regulating radial glia neural stem cells (RGCs) in the developing mouse cortex in vivo. This, in turn, led to targeted human genetic association analyses, resulting in the identification of an epistatic interaction for risk of schizophrenia. Our integrated analyses from multiple systems provide insight into how 15q11.2 CNVs may contribute to defects in neural development and brain disorders.

RESULTS

Defects in Adherens Junctions and Apical Polarity of hNPCs Derived from Human iPSCs Carrying 15q11.2 Del

To determine how 15q11.2 del may affect human brain development, we established multiple iPSC lines from skin fibroblasts of three individuals carrying 15q11.2 del in one chromosome (Y1, Y3, and Y4) and from three control individuals (C1, C2, and C3) using nonintegrating approaches (Figure 1C; Table S1 available online). We performed detailed quality control analyses of all iPSC lines selected for the current study (Table S1). These iPSCs maintained embryonic stem cell-like morphology, expressed pluripotency-associated markers, and exhibited normal euploid karyotypes (Figures 1C and S1; Tables S1 and S2). All iPSC lines tested formed teratomas when injected into severe combined immunodeficiency (SCID) mice (Table S1). We also included iPSC lines from two neuropsychiatric patients with a DISC1 mutation as another group for comparison (D2 and D3) (Chiang et al., 2011). Using DNA fluorescence in situ hybridization (FISH), we confirmed one copy microdeletion at 15q11.2 locus in Y1, Y3, and Y4, but not in other fibroblasts and iPSC lines we examined (C1, C2, C3, D2, D3) (Figures 1A and 1D; Table S1).

We first differentiated iPSCs into relatively homogenous primitive neural precursor cells (pNPCs) in monolayer using an established protocol (Li et al., 2011). All lines were efficiently differentiated into pNPCs expressing NESTIN and SOX2 (Figure S2A). No consistent differences in the NPC differentiation efficacy or proliferation among different groups of iPSC lines were detected (Figures S2A and S2B). To partially maintain cell-cell interaction, we next generated cortical neural rosettes using small molecule inhibitors and retinoic acid (Shi et al., 2012). We initially used four iPSC lines for pilot phenotypic characterization, including one iPSC line each from two control subjects (C2-1 and C3-1) and two lines from one subject with 15q11.2 del (Y1-1 and Y1-3). Neural rosettes from C2-1 and C3-1 iPSCs showed robust expression of atypical PKCλ, an apical polarity marker, as a ring-like structure at the luminal surface of each rosette (Figure 1E), representing typical formation of apical-basal polarity of hNPCs (Shi et al., 2012). Interestingly, the majority of neural rosettes from Y1-1 and Y1-3 iPSCs exhibited scattered expression of atypical PKCλ (Figure 1E). The structure of adherens junctions as revealed by N-cadherin immunostaining was also disrupted in the majority of rosettes from two Y1-iPSC lines (Figure 1F). These results suggest that gene(s) located within 15q11.2 del regulate apical polarity and maintain adherens junctions of hNPCs.

WAVE Complex Destabilization and Polarity Defects of hNPCs Due to CYFIP1 Haploinsufficiency

The actin cytoskeleton acts as a cytoplasmic anchor for cadherin/catenin proteins at adherens junctions and its proper organization is important for maintaining adherens junctions and polarity of neural precursors in the developing mouse cortex (Buchman and Tsai, 2007). Among the four genes within the 15q11.2 region, CYFIP1 is a regulator of the actin-modulating WAVE complex (Kunda et al., 2003; Steffen et al., 2004). Indeed, coimmunoprecipitation (co-IP) analysis showed that CYFIP1 interacts with WAVE complex components WAVE1, WAVE2, and NAP1 (NCKAP1) in normal hNPCs (Figure 2A). Therefore, we assessed WAVE complex integrity in hNPCs derived from different iPSC lines. Consistent with a haploinsufficiency model, mRNAs of all four genes within 15q11.2 were expressed at ~50% levels in all hNPCs carrying 15q11.2 del compared to those without the deletion (Figure S2C). CYFIP1 protein was also expressed at ~50% levels (Figures 2B, 2D, and S2D). Strikingly, the expression of WAVE2 protein, but not its mRNA, in 15q11.2 del hNPCs was only ~20% of that in control hNPCs (Figures 2B, 2E, and S2D). The effect of 15q11.2 microdeletion appeared to be specific, as hNPCs derived from mutant DISC1-iPSC lines showed normal expression of CYFIP1 and WAVE2 proteins (Figures 2D, 2E, and S2D). Together, these biochemical analyses demonstrated a specific defect of WAVE complex stabilization in hNPCs with 15q11.2 microdeletion.

Is *CYFIP1* haploinsufficiency the major cause of observed defects in hNPCs carrying 15q11.2 del? First, we performed complementation experiments using lentiviruses to increase CYFIP1 levels in two Y1-iPSC lines. We selected two iPSC lines that gave rise to hNPCs with the total amount of CYFIP1 protein at comparable levels to C3-1 hNPCs (Y1-1-CP and Y1-3-CP; Figures 2B and 2D). Importantly, the WAVE2 protein level in these complemented lines was fully rescued (Figures 2B and 2E), suggesting that *CYFIP1* haploinsufficiency is required for WAVE complex destabilization in hNPCs with 15q11.2 del. Second, to determine whether decreased CYFIP1 expression is sufficient to cause WAVE complex destabilization in hNPCs, we reduced the endogenous CYFIP1 protein level in control hNPCs to ~50% with short hairpin RNA (shRNA) (Figure 2C; Table S3). Indeed, expression of shRNA-*CYFIP1*, but not shRNA-control, led to significantly decreased WAVE2 protein expression (Figure 2C). Finally, we examined whether *CYFIP1* haploinsufficiency is the cause of adherens junction and apical polarity impairments observed in neural rosettes from hNPCs with 15q11.2 del. We first validated our pilot results using an independent embryoid body protocol (Juopperi et al., 2012), which gave rise to pure $PAX6^+$ neural progenitors (Figure S2E). Scattered expression of atypical PKCλ at the luminal surface was observed for the majority of neural rosettes from multiple iPSC lines with 15q11.2 del (Figures 2F and 2G). Importantly, complementation of CYFIP1 expression to the normal level in two Y1 lines rescued the expression of atypical PKCλ at the luminal surface (Figures 2F and 2G), whereas reduction of CYFIP1 expression by shRNA in C3-1 hNPCs led to scattered expression of atypical PKCλ (Figure S2F). Consistent with an intact WAVE complex, neural rosettes derived from mutant DISC1-iPSCs exhibited normal distribution of PKCλ at the luminal surface (Figure 2G). Analysis of additional polarity markers, including PAR3 and β-catenin, also showed consistent results across the groups (Figure S2G).

Taken together, this series of biochemical and functional analyses of a collection of 20 iPSC lines established that 15q11.2

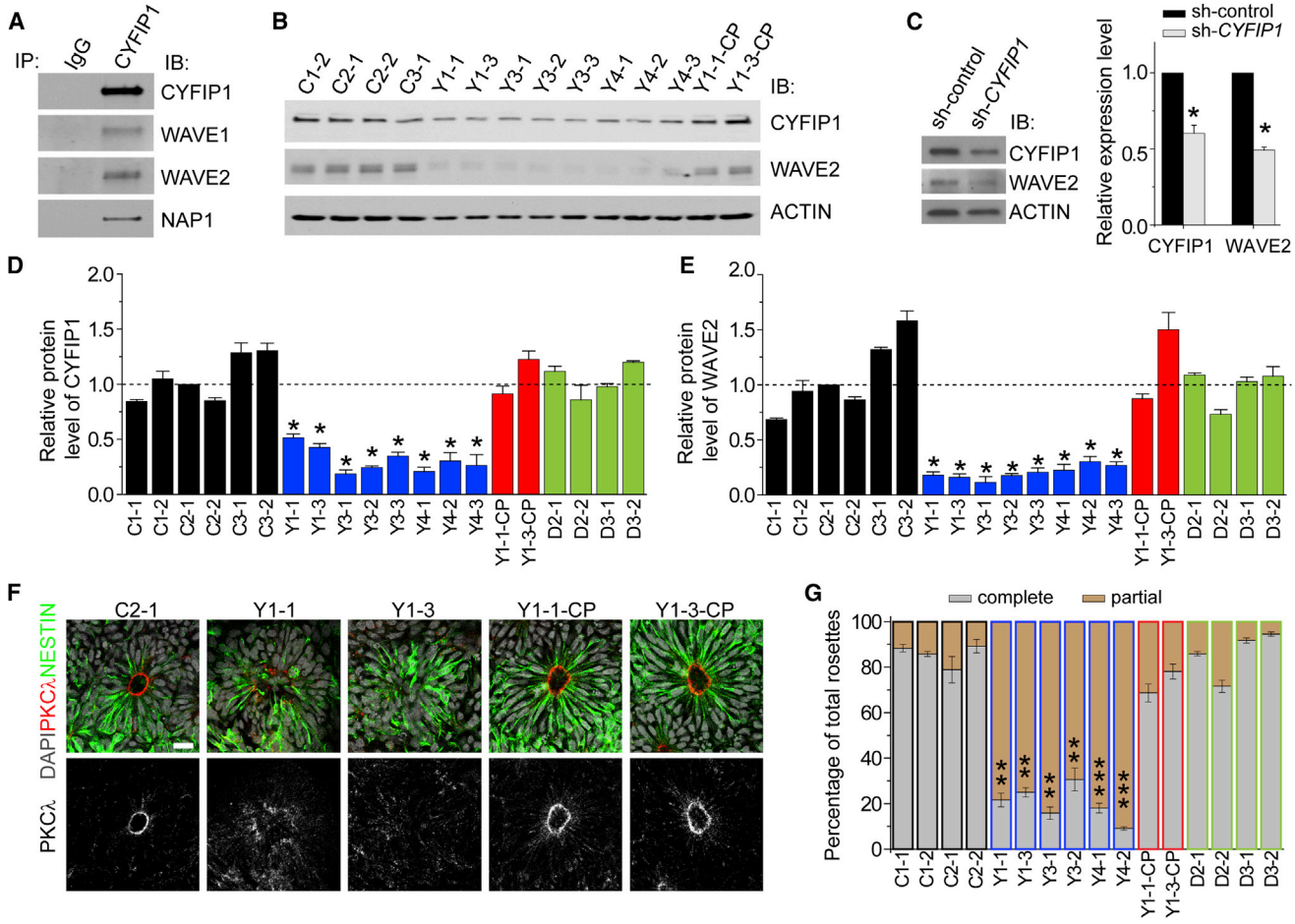

Figure 2. Destabilization of the WAVE Complex and Polarity Defects of hNPCs Due to CYFIP1 Deficiency

(A) CYFIP1 is a component of WAVE complex in human pNPCs. Shown are sample western blot images of co-IP analysis of pNPCs using anti-CYFIP1 antibodies.

(B) Reduced CYFIP1 and WAVE2 protein levels in pNPCs carrying 15q11.2 del. Lentiviruses were used to establish two CYFIP1 complementation lines (Y1-1-CP and Y1-3-CP).

(C) Decreased WAVE2 protein levels after CYFIP1 knockdown by lentivirus-mediated shRNA expression in normal pNPCs for 48 hr.

(D and E) Quantification of protein levels of CYFIP1 and WAVE2 among different pNPCs. All data were normalized to ACTIN levels for loading control and then normalized to CYFIP1 (D) or WAVE2 (E) in C2-1 pNPCs for comparison. Values represent mean ± SEM (n = 3–5 cultures; *p < 0.05; Student's t test).

(F and G) Defect in adherens junctions and apical polarity of hNPCs carrying 15q11.2 del and its rescue by CYFIP1 complementation. Shown on the left are sample confocal images of immunostaining of atypical PKCλ for neural rosettes differentiated from iPSCs using the embryoid body method. Scale bar represents 20 μm. Shown on the right are quantifications of neural rosettes similar as in Figure 1E. Values represent mean ± SEM (n = 5 cultures; ***p < 0.001; **p < 0.01; Student's t test). See also Figure S2 and Tables S1 and S3.

del, through CYFIP1 deficiency, leads to defects in the maintenance of adherens junctions, apical polarity, and WAVE complex stability in hNPCs.

Requirement of CYFIP1 in Maintaining Adherens Junctions and Apical Polarity of RGCs in Developing Mouse Cortex

Given limitations of in vitro studies of human iPSCs, we next turned to in vivo mouse embryonic cortical development to assess whether the CYFIP1 function we identified in regulating hNPCs is physiologically relevant in vivo and, furthermore, to examine the long-term consequence of CYFIP1 deficiency in cortical development. In the E15.5 dorsal neocortex, CYFIP1 was found to be accumulated at the ventricular surface in the ventricular zone (VZ), with lower expression in migrating neurons in the intermediate zone (IZ) (Figure 3A). The VZ of the midneurogenic period is mostly occupied by RGCs, which are neural stem cells in the developing cortex (Kriegstein and Alvarez-Buylla, 2009). The apical processes of adjacent RGCs are attached to one another via cadherin-based adherens junctions at the ventricular surface (Loulier et al., 2009; Rasin et al., 2007). Coimmunostaining showed that CYFIP1 was highly expressed at the F-actin-expressing lateral membrane domain and N-cadherin- and β-catenin-expressing adherens junctions in the apical endfeet of RGCs (Figures 3B and 3C). With an en face view from the ventricle, CYFIP1 was found as cytosolic puncta inside of the ring-like F-actin structure on the ventricular surface (Figure 3C).

To investigate CYFIP1 function in regulating RGCs, we generated effective shRNAs specifically against mouse *Cyfip1*

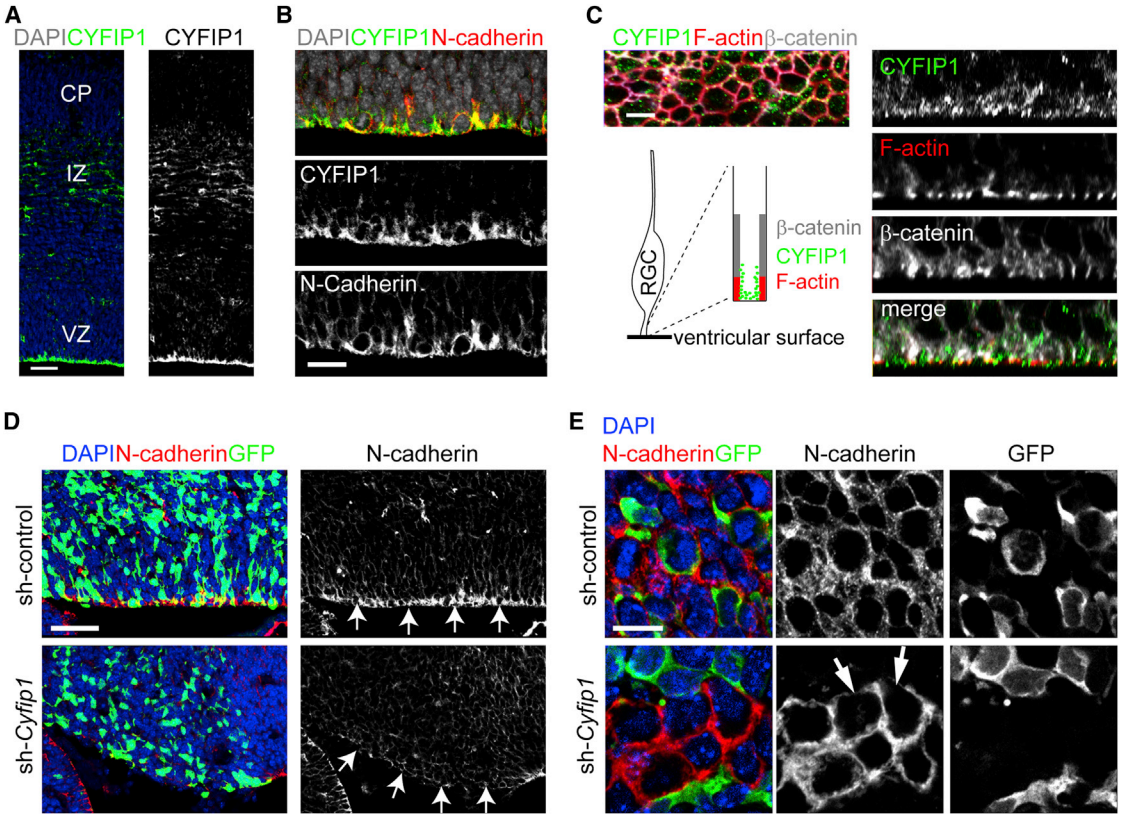

Figure 3. Critical Role of CYFIP1 in Regulating Adherens Junctions and Apical Polarity of RGCs in the Developing Mouse Cortex

(A–C) Expression of CYFIP1 in the mouse neocortex at E15.5. Shown are sample confocal images of immunostaining of CYFIP1 and N-cadherin. VZ, ventricular zone; IZ, intermediate zone; CP, cortical plate. Also shown is the en face view of CYFIP1 expression at the ventricular surface (C, left panel). The structure of F-actin, which forms the boundary between apical endfeet of RGCs on the ventricular surface, was labeled by Phalloidin-Alexa594 (Red). Cross-section images are shown in right panels. Scale bars represent 50 μm (A), 20 μm (B), and 5 μm (C).

(D and E) Expression of CYFIP1 and other apically polarized proteins in the mouse neocortex at E16.5 after in utero electroporation at E13.5 to coexpress GFP and sh-control or sh-*Cyfip1* (#2). Shown are sample confocal images of immunostaining for GFP and N-cadherin (D) and the en face view at 3 μm from the ventricular surface (E). Scale bars represent 50 μm (D) and 10 μm (E).

See also Figure S3 and Tables S2 and S3.

(Figure S3A; Table S3). We performed in utero electroporation with vectors coexpressing GFP and shRNA-*Cyfip1#2* (sh-*Cyfip1*), or control shRNA (sh-control), into the E13.5 neocortex, and analyzed 3 days later. GFP$^+$ cells expressing sh-*Cyfip1* showed largely absent CYFIP1 immunoreactivity, confirming the shRNA efficiency against endogenous CYFIP1 in vivo (Figure S3B). While GFP$^+$ cells expressing sh-control in the VZ showed robust N-cadherin expression at the ventricular surface, those expressing sh-*Cyfip1* did not (Figures 3D and 3E). En face view near the ventricular surface further showed reduced N-cadherin expression in some GFP$^-$ cells at regions in contact with GFP$^+$ cells expressing sh-*Cyfip1*, suggesting a potential noncell autonomous effect (Figure 3E). Thus, similar to its function in cultured hNPCs, CYFIP1 maintains adherens junctions and apical polarity of neural stem cells in the developing mouse cortex in vivo.

Ectopic Localization of CYFIP1-Deficient RGCs outside of the VZ

What is the functional consequence of impairments in adherens junctions and apical polarity of RGCs from CYFIP1 deficiency? We examined RGC cell body distribution by Pax6 immunohistochemistry. Pax6$^+$GFP$^+$ cells expressing sh-control were mostly restricted within the VZ (Figures 4A, left panel, and 4B). In contrast, a significant percentage of Pax6$^+$GFP$^+$ cells expressing sh-*Cyfip1* (#2) were ectopically misplaced in the subventricular zone (SVZ) and IZ, at the expense of VZ localization (Figures 4A, middle panel, and 4B). Aberrant localization of RGCs was also observed with an independent shRNA against mouse *Cyfip1* (#1; Figure S4A). Importantly, this defect was rescued by coexpression of shRNA-resistant CYFIP1 cDNA (Figures 4A, right panel, and 4B), confirming the specificity of shRNA experiments.

GFP$^+$ mitotic cells labeled with phospho-HistoneH3 were also found to be scattered in the SVZ and IZ (Figure 4C). To determine whether NPC proliferation was affected by CYFIP1 deficiency, proliferating cells were pulsed with EdU and examined 2 hr later. Similar to hNPCs in vitro (Figure S2B), CYFIP1-deficient cells showed EdU incorporation comparable to those expressing sh-control, despite their ectopic localization (Figures 4D and S4B). To examine cell cycle progression, we determined the cell-cycle exit index defined as the percentage of EdU$^+$Ki67$^-$ cells among all EdU$^+$ cells at 24 hr after EdU administration and did not find

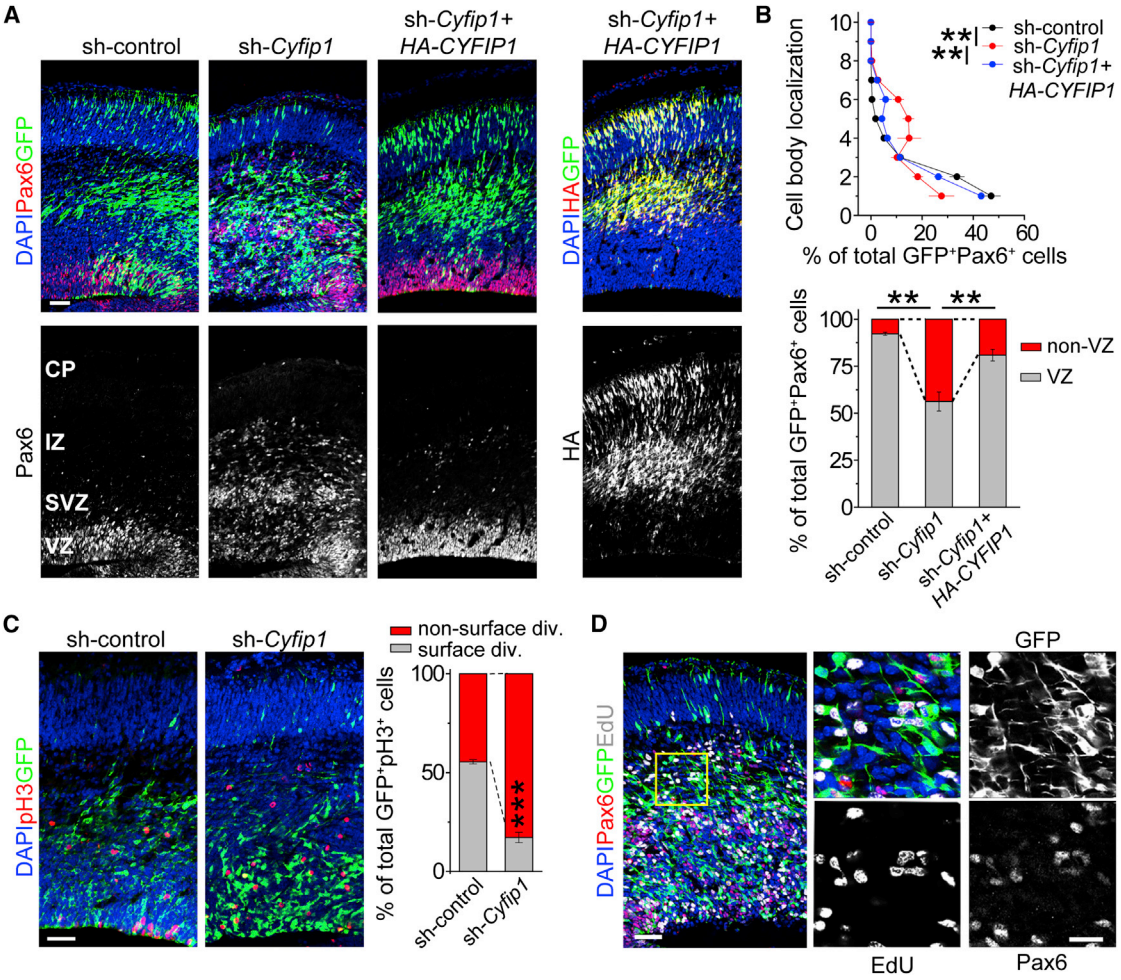

Figure 4. Ectopic Localization of CYFIP1-Deficient RGCs outside of the VZ in the Developing Mouse Cortex

(A and B) Ectopic localization of Pax6$^+$ RGCs in the SVZ and IZ of E16.5 neocortices after in utero electroporation at E13.5 to coexpress GFP and sh-control or sh-*Cyfip1*, or coexpress GFP/sh-*Cyfip1* and cDNA for shRNA-*Cyfip1* resistant HA-tagged CYFIP1. Shown in (A) are sample confocal images of immunostaining of Pax6, GFP, and HA. Cotransfection of GFP/sh-*Cyfip1* and shRNA-resistant HA-tagged CYFIP1 was confirmed by colocalization of GFP and HA immunostaining (the right-most panel). Scale bar represents 50 μm. Shown in (B) are two different quantifications of the distribution of GFP$^+$Pax6$^+$ cells in the neocortex. Upper panel represents GFP$^+$Pax6$^+$ cells in each of ten equal-size vertical bins expressed as percentages of total GFP$^+$Pax6$^+$ cells (1: the most apical, 10: the most basal). Lower panel represents percentages of GFP$^+$Pax6$^+$ cells in the VZ (VZ) and in other layers (non-VZ). Values represent mean ± SEM (n = 4–5 animals; **p < 0.01; Student's t test).

(C) Aberrant localization of proliferating cells expressing sh-*Cyfip1* in E16.5 neocortex. Sample confocal images of immunostaining for GFP and an M-phase marker, phospho-HistoneH3 (pH3), are shown. Scale bar represents 50 μm. Also shown are quantifications of percentages of GFP$^+$pH3$^+$ cells at the ventricular surface (surface division) and at other locations (nonsurface division). Values represent mean ± SEM (n = 5 animals; ***p < 0.001; Student's t test).

(D) Proliferation of CYFIP1-deficient RGCs outside of the VZ. E13.5 embryos were electroporated to coexpress GFP and sh-*Cyfip1* and fixed at 2 hr after EdU injection at E16.5. Shown are sample confocal images of staining for GFP, Pax6, EdU, and DAPI. Note that ectopic GFP$^+$Pax6$^+$ cells in the IZ still incorporated EdU, representing their ability to proliferate far from the ventricular surface. Scale bars represent 50 μm (left panel) and 20 μm (insets).

See also Figure S4 and Table S2.

any differences (Figure S4C). Together, these results indicate that CYFIP1 is important for proper placement and pattern of mitosis, but not essential for the proliferation and cell-cycle progression of RGCs in the developing mouse cortex in vivo.

Ectopic Placement of Intermediate Progenitor Cells and Cortical Neurons Generated from CYFIP1-Deficient RGCs

We next examined the direct progeny from RGCs, intermediate progenitor cells (IPCs), which express Tbr2 and proliferate transiently in the SVZ to generate neurons (Englund et al., 2005). Tbr2$^+$GFP$^+$ cells expressing sh-*Cyfip1* were also scattered in the VZ/SVZ/IZ, while Tbr2$^+$GFP$^+$ cells expressing sh-control mainly resided in the SVZ (Figures 5A and 5B). On the other hand, the proportion of Pax6$^+$GFP$^+$ cells and Tbr2$^+$GFP$^+$ cells were not altered between those expressing sh-control and sh-*Cyfip1* (Figure 5C), suggesting that CYFIP1 is dispensable for the proper differentiation of RGCs into IPCs.

Glutamatergic projection neurons of the adult cortex are generated in a stereotyped temporal order, with deep layer

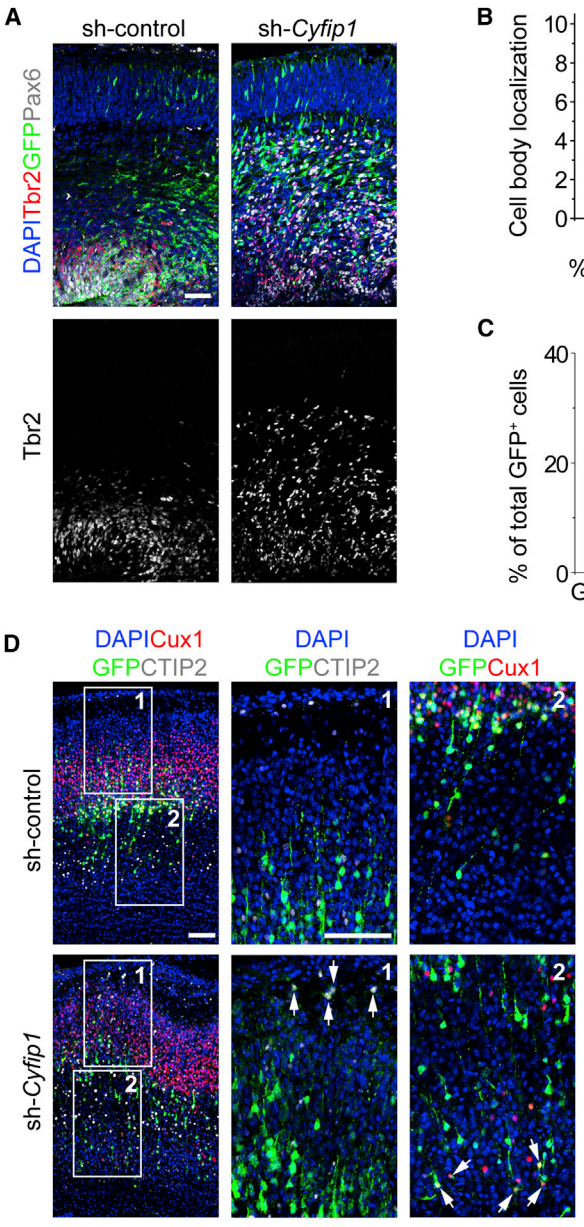

Figure 5. Ectopic Placement of Intermediate Progenitor Cells and Cortical Neurons upon CYFIP1 Knockdown in RGCs

(A–C) Ectopic placement of intermediate progenitor cells (IPCs) upon CYFIP1 knockdown in RGCs. E13.5 embryos were electroporated to coexpress GFP and sh-*Cyfip1* or sh-control and examined at E16.5. Shown in (A) are sample confocal images of immunostaining for GFP, Pax6, Tbr2, and DAPI. Scale bar represents 50 μm. Shown in (B) are quantifications of the distribution of GFP^+Tbr2^+ cells in the neocortex. The graph represents GFP^+Tbr2^+ cells in each of ten equal-size vertical bins expressed as the percentage of total GFP^+Tbr2^+ cells. Values represent mean ± SEM (n = 4–5 animals; $^{**}p < 0.01$; Student's t test). Shown in (C) are quantifications of percentages of GFP^+ cells that were $Pax6^+$ or $Tbr2^+$. Values represent mean ± SEM (n = 4 animals; $p > 0.1$; Student's t test).

(D and E) Ectopic placement of cortical neurons upon CYFIP1 knockdown in RGCs. Same as in (A–C), except that electroporated brains were examined at P5. Shown in (D) are sample confocal images of immunostaining for GFP, Cux1, and CTIP2. Right panels represent two different insets in the left panels. Arrows point to GFP^+CTIP2^+ or GFP^+Cux1^+ cells. Scale bars represent 100 μm. Shown in (E) are quantifications of percentages of GFP^+CTIP2^+ cells (top panel) or GFP^+Cux1^+ cells (bottom panel) that were distributed in upper or deep layers, respectively. The boundary between upper and deep layers was established at the apical limit of $Cux1^+$ cells. Values represent mean ± SEM (n = 4 animals; $^*p < 0.05$; Student's t test).

See also Table S2.

neurons (layer V/VI: $CTIP2^+$) produced first and upper layer neurons (layer II/III/IV: $Cux1^+$) produced later (Leone et al., 2008). Defects in RGCs, which serve as the main radial scaffold for migrating neurons, could potentially lead to failure of neurons to reach their normal position. To examine the long-term consequence of *Cyfip1* knockdown on cortical layer formation, we analyzed P5 brains after in utero electroporation of shRNAs at E13.5. $CTIP2^+$ neurons, which normally localize in deep layers, showed more frequent localization in upper layers after sh-*Cyfip1* expression in RGCs (Figures 5D and 5E). On the contrary, $Cux1^+$ neurons, which normally localize in upper layers, were present in a higher percentage in deep layers after sh-*Cyfip1* expression (Figures 5D and 5E). The ratio of $CTIP2^+$ versus $Cux1^+$ cells among all GFP^+ cells was not significantly different between sh-control (0.22 ± 0.03) and sh-*Cyfip1* (0.23 ± 0.02; n = 4), suggesting that CYFIP1 is dispensable for neuronal subtype specification. Some mislocalized $Cux1^+$ and $CTIP2^+$ cells appeared to be GFP^- (Figure 5D). This could be due to the diluted GFP expression in the P5 brain after multiple rounds of cell division or, alternatively, noncell autonomous migration defects due to aberrant radial scaffolds of CYFIP1-deficient RGCs. These results demonstrate that CYFIP1 deficiency causes improper placement of IPCs and glutamatergic projection neurons, resulting in cortical layer malformation.

CYFIP1 Signaling Mechanism in Regulating RGCs in the Developing Embryonic Mouse Cortex

Similar to findings from hNPCs (Figure 2A), co-IP analysis using E14.5 mouse cortical lysates showed that endogenous CYFIP1 interacted with several WAVE components, including WAVE1, WAVE2, Abi1, and Nap1 (Figure 6A). Knockdown of CYFIP1 in mouse NPCs in vitro also led to marked decrease of WAVE2 and Abi1 proteins (Figure 6B). Immunohistological analysis showed that WAVE2 protein expression at the ventricular surface was drastically decreased after *Cyfip1* knockdown in vivo (Figure 6C). These results suggested a conserved role and

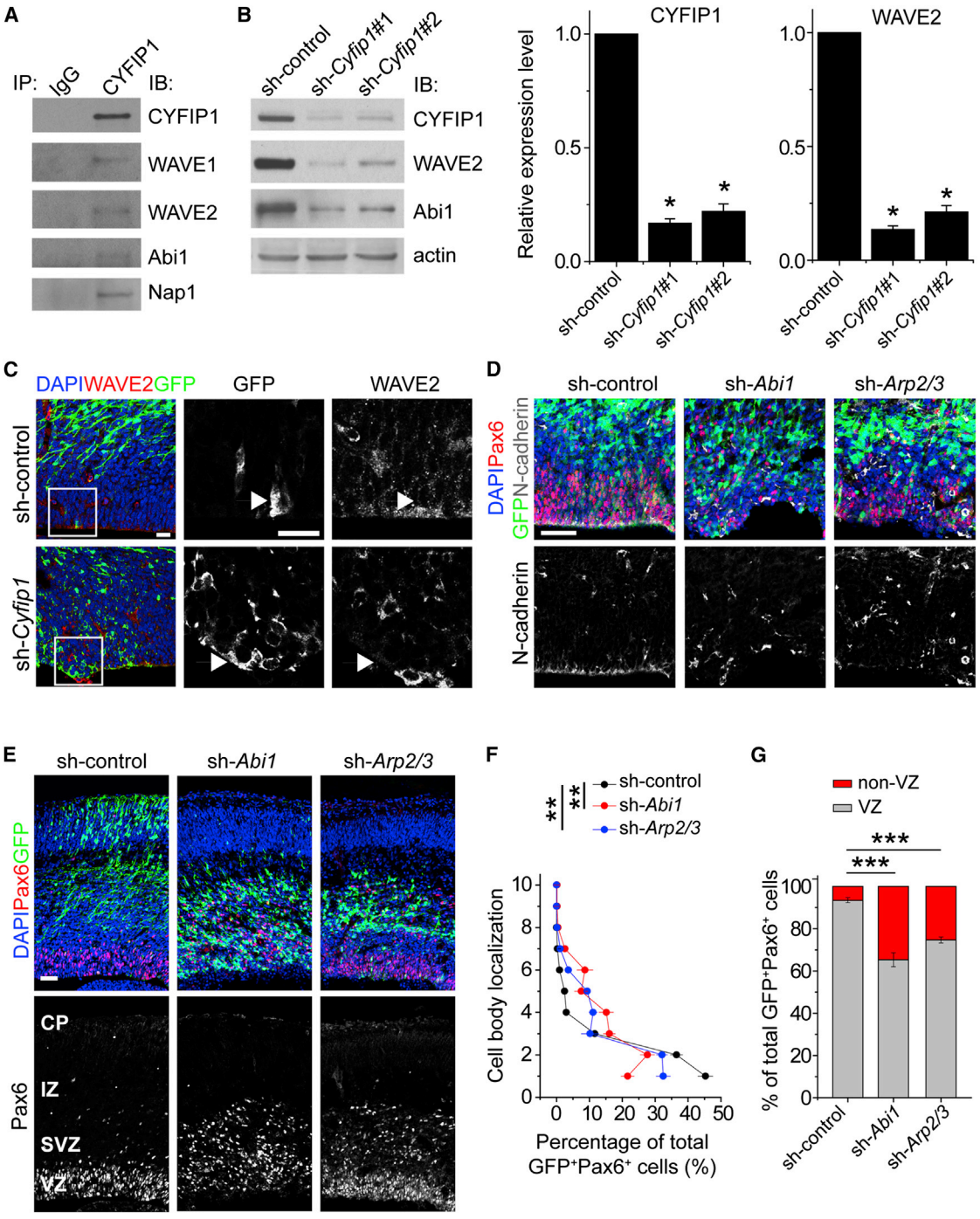

Figure 6. Critical Role of CYFIP1 Signaling in Maintaining Adherens Junctions and Proper Placement of RGCs in the Developing Mouse Cortex

(A) CYFIP1 is a component of WAVE complex in the developing mouse cortex. Shown are sample western blot images of co-IP analysis using anti-CYFIP1 antibodies and E14.5 forebrain lysates.

(B) Reduced WAVE2 protein levels by CYFIP1 knockdown in mouse NPCs. Mouse NPCs were infected with retroviruses expressing sh-control, or sh-*Cyfip1* (#1 or #2) and then subjected to western blot analyses 3 days later. Shown are sample western blot images and quantifications of CYFIP1 and WAVE2 protein levels. Values represent mean ± SEM (n = 3; **p < 0.01; Student's t test).

(C) Reduced WAVE2 protein levels at the ventricular surface in E16.5 neocortices in vivo. E13.5 embryos were electroporated to coexpress GFP and sh-*Cyfip1* or sh-control and examined at E16.5. Shown are sample confocal images of immunostaining for GFP, WAVE2, and DAPI. Scale bar represents 20 μm.

(D–G) Similar RGC defects among knockdown of CYFIP1, WAVE complex component Abi1, or downstream effectors Arp2/3. E13.5 embryos were electroporated to coexpress GFP and sh-*Abi1* or sh-*Arp2*/sh-*Arp3* (double knockdown), and examined at E16.5. Shown in (D) are sample confocal images of immunostaining for

(legend continued on next page)

signaling mechanism of CYFIP1 in regulating WAVE complex stability and adherens junctions in both human and mouse NPCs.

Next, we examined the functional role of CYFIP1-dependent WAVE complex and downstream signaling in regulating RGCs in vivo (Figure S5A). We developed effective shRNAs against mouse *Abi1* and downstream mediators *Arp2/3* (Figures S5B and S5C). In utero electroporation analyses showed a lack of N-cadherin expression at the ventricular surface by GFP^+ cells expressing sh-*Abi1* or sh-*Arp2/3* (double knockdown; Figure 6D). GFP^+Pax6^+ cells expressing sh-*Abi1* or sh-*Arp2/3* also showed scattered distribution in the VZ/SVZ/IZ (Figures 6E–6G). These results suggest that, similar to CYFIP1, WAVE complex-mediated signaling is important for the maintenance of adherens junctions and proper placement of RGCs in the developing cortex.

Epistatic Interaction of Gene Expression-Associated Variants of the WAVE Signaling Components for Risk of Schizophrenia

Our findings of similar roles of WAVE signaling components in regulating RGCs, together with previous findings of association of 15q11.2 del with risk for schizophrenia (Malhotra and Sebat, 2012), led to a hypothesis that common genetic variants within the WAVE signaling pathway might interact to affect risk for schizophrenia even in the absence of association at the individual gene level (Figure 1B). The goal of the clinical genetic association analyses was to model molecular interactions of CYFIP1 and WAVE components identified in iPSC and animal studies. We first examined mRNA expression in the dorso-lateral prefrontal cortex (DLPFC) of postmortem human brains in order to find specific genetic variants that were associated with expression of genes in the WAVE signaling pathway (i.e., expression quantitative trait loci [eQTLs]). We performed a *cis*-association analysis of SNP variants with gene expression measured by RNA-sequencing (RNA-seq) in a group of 64 Caucasian subjects with no history of medical or psychiatric disease (Table S4). Significant associations were found for rs268864 with *ACTR2*/*Arp2* expression ($p = 0.02$), rs2797930 with *ABI1* expression ($p = 0.02$), and rs7168367 with *CYFIP1* expression ($p = 0.006$). SNP rs4778334, previously associated with risk for schizophrenia in a case-control Han Chinese sample (Zhao et al., 2013a), was also associated with *CYFIP1* gene expression ($p = 0.05$). Interestingly, rs4778334 does not show linkage disequilibrium with other genotyped SNPs in the European ancestry populations or in the Chinese, consistent with a potential functional effect of this SNP (Figure S6). We also found that, except for *CYFIP1*, all genes in this network (*ABI1*, *WASF1*/*WAVE1*, *WASF2*/*WAVE2*, *NCKAP1*/*Nap1*, *ACTR2*/*Arp2*, and *ACTR3*/*Arp3)* tend to be coexpressed together in a similar pattern (Table S5).

To search for evidence that eQTLs in the WAVE signaling pathway might be associated with risk for schizophrenia, we performed single genetic association analysis of the selected four expression-associated SNPs (or proxy SNPs) in four independent schizophrenia case-control data sets of European ancestry. No significant single SNP association was found in any of the four cohorts (Table S6). Targeted pairwise SNP-SNP interaction analyses were carried out among three SNPs—rs268864 (SNP1) at *ACTR2*, rs4778334 (SNP3) at *CYFIP1||NIPA2*, and rs7168367 (SNP4) at *CYFIP1||NIPA1* as these were only SNPs genotyped in all four cohorts. An interaction was detected between rs268864 at *ACTR2* and rs4778334 at *CYFIP1||NIPA2* at a marginal significance ($p = 0.0553$) in the largest American LIBD/CBDB cohort (Figure 7A). The same trend of interaction with these exact alleles was also found in three smaller schizophrenia case-control cohorts of American (GRU; $p = 0.149$), German (MUN; $p = 0.258$), and Scottish origin (ABE; $p = 0.215$). Meta-analysis of the pairwise interaction in all four cohorts showed significant evidence for interaction ($p = 0.00417$) between rs268864 at *ACTR2* and rs4778334 at *CYFIP1||NIPA2;* interaction analysis of the combined sample of four cohorts confirmed the interaction in both an additive model ($p = 0.0035$) and a genotypic model ($p = 0.0048$; Figure 7A). The results of the meta-analysis are significant after correction for all combinations of two-way interactions based on the three SNPs analyzed. Moreover, the interactions, which were directionally consistent across all four data sets, were hypothesized based on eQTLs that specifically modeled the directionality of biologic interactions in the model system experiments.

It is interesting to note that depending on the genotype background of the *ACTR2* SNP rs268864, genotypes of rs4778334 at *CYFIP1* showed varying effects from negative to positive on risk of schizophrenia (Figure 7B). In the group of rs268864 genotype AA, individuals carrying genotype CC and CT at rs4778334 were less likely associated with risk of schizophrenia in comparison with TT genotype ($p = 0.0244$), and odds ratio estimates were 0.716 and 0.772, respectively. In contrast, in the group of rs268864 genotype GG, individuals carrying genotype CC and CT at rs4778334 were more likely associated with risk of schizophrenia in comparison with TT genotype ($p = 0.0103$), and odds ratio estimates were 11.14 and 4.56, respectively. Alternating genotype associations at one locus based on the genotype at another locus are classic epistatic phenomena.

DISCUSSION

Our study identified the functional role and signaling mechanism underlying CYFIP1 regulation of neural stem cells and provides insight into how risk factors for neuropsychiatric disorders regulate neural development. Using human iPSCs as an entry point to investigate a prominent CNV risk factor encompassing multiple genes for schizophrenia and other neuropsychiatric disorders (Figures 1A and 1B), we uncovered cellular phenotypes in derived hNPCs and identified the responsible gene within the CNV. These in vitro findings of developmentally relevant phenotypes in human cells guided our analyses of neural stem cells in the developing mouse cortex in vivo and led to the identification of the underlying signaling mechanism. The mechanistic insight

GFP, Pax6, N-cadherin, and DAPI. Shown in (E) are sample confocal images of immunostaining for GFP, Pax6, and DAPI. Scale bars represent 50 μm. Also shown are two different quantifications of the distribution of GFP^+Pax6^+ cells in the neocortex among different experiments, similar as in Figure 4B. Values represent mean ± SEM ($n = 4$ animals; $^{**}p < 0.01$; $^{***}p < 0.001$; Student's t test).
See also Figure S5 and Tables S2 and S3.

A

Effect	DF	Wald Chi-Square	p
American (LIBD/CBDB)	1	3.6722	0.0553
American (GRU)	1	2.0817	0.1491
German (MUN)	1	1.2778	0.2583
Scottish (ABE)	1	1.5369	0.2151
Combined sample:			
Additive model	1	8.5387	0.0035
Genotypic model	4	14.9641	0.0048

B

	*CYFIP1//NIPA1**rs4778334							95% Confidence Limit		
*ACTR2**rs268864	Genotype	Reference	Estimate	SE	P	Adj P	OR	Lower	Upper	p*
AA(=0)										0.0244
	CC(=0)	TT	-0.3343	0.1246	0.0073	0.0219	0.716	0.561	0.914	
	CT(=1)	TT	-0.2588	0.1270	0.0416	0.1248	0.772	0.602	0.990	
AG(=1)										0.4976
	CC(=0)	TT	0.1524	0.2080	0.4638	1	1.165	0.775	1.751	
	CT(=1)	TT	0.2359	0.2130	0.2680	0.8040	1.266	0.834	1.922	
GG(=2)										0.0103
	CC(=0)	TT	2.4106	1.0979	0.0281	0.0844	11.140	1.295	5.821	
	CT(=1)	TT	1.5172	1.1101	0.1717	0.5152	4.560	0.518	40.166	

Figure 7. Epistatic Interaction of Gene Expression-Associated Variants of the WAVE Signaling Components for Risk of Schizophrenia

(A) Interaction analysis of SNPs rs2688674**ACTR2* and rs4778334**CYFIP1-NIPA1* in combined samples of four cohorts in European ancestry population. Analysis was performed adjusting for sex and cohort effect. DF, degree of freedom.

(B) Effect of interaction by genotypes on risk of schizophrenia from a logistic regression model based on genotypic interaction of *ACTR2* and *CYFIP1* in combined samples of four cohorts. Adj p is p value after adjusting for multiple testing from post hoc analysis. SNPs were coded as 0, 1, and 2 for number of minor alleles. See also Figure S6 and Tables S4, S5, and S6.

allowed us to generate a hypothesis and test it with gene expression analyses in human brains and genetic association studies, resulting in the identification of an epistatic interaction for risk of schizophrenia. Our study provides an example of how genetic risk factors for complex human disorders can be studied in complementary systems using patient-derived iPSCs as the leading tool for discovery.

15q11.2 CNVs have emerged as a prominent risk factor for several neuropsychiatric disorders (Malhotra and Sebat, 2012). Our results from multiple levels of analyses provide evidence to support a specific gene within this CNV, CYFIP1, as a potential major contributing factor to biological processes implicated in the neurodevelopmental origins of these disorders. 15q11.2 del has been identified as one of the three most frequent CNV risk factors for schizophrenia and increases risk 2- to 4-fold (International Schizophrenia Consortium, 2008; Stefansson et al., 2008). While none of the SNPs we examined within the CYFIP1 and WAVE signaling pathway showed significant independent risk for schizophrenia in four cohorts of European ancestry, we identified a potential epistatic interaction between *CYFIP1* and WAVE signaling mediator *ACTR2 /Arp2* for increased risk for schizophrenia with an odds ratio up to 11 (Figure 7B). While these results must be taken as preliminary and in need of further replication as the overall statistics are not particularly strong, our study implicates WAVE signaling in risk for schizophrenia and supports an emergent model that multiple factors within the same signaling pathway interact epistatically to affect the risk for psychiatric disorders. Notably, 15q11.2 CNVs themselves are not specific to schizophrenia (De Wolf et al., 2013). In a large study with over 15,000 patient samples, 15q11.2 del was found to be strongly associated with developmental delay in children (Cooper et al., 2011). Studies have also linked 15q11.2 del to epilepsy (de Kovel et al., 2010; Jähn et al., 2014; Mullen et al., 2013). Interestingly, CNVs with a duplication of this same region have been associated with autistic spectrum disorder (Nishimura et al., 2007; van der Zwaag et al., 2010; Wegiel et al., 2012). In addition, CYFIP1 is within larger 15q11.2-13.1 CNVs that have also been linked to schizophrenia, autistic spectrum disorder, and bipolar disorder (Malhotra and Sebat, 2012). Therefore, our findings have broad implications for these disorders and identify a signaling pathway for future targeted investigation.

Our study provides insight into how CYFIP1 signaling regulates early mammalian neural development. While several previous studies have investigated roles of CYFIP1 in neurons, its function in neural stem cells was completely unknown. In *Drosophila*, the fly ortholog of *Cyfip1* was shown to regulate neuromuscular junction formation (Schenck et al., 2003; Zhao et al., 2013b) and eye morphogenesis (Bogdan et al., 2004; Galy et al., 2011). In mice, CYFIP1 interacts with FMRP and cap protein eIF4E to regulate activity-dependent protein translation in mature neurons (Napoli et al., 2008). Furthermore, *Cyfip1* haploinsufficiency in mice produces fragile X-like phenotypes (Bozdagi et al., 2012). By focusing on the earliest stages of cortical development, our study provides evidence for a critical role of CYFIP1 in regulating adherens junctions and apical polarity of both human neural stem cells in the neural rosette model and mouse RGCs in the developing cortex in vivo. Moreover, as a functional consequence of CYFIP1 deficiency, RGCs and their progeny are aberrantly localized in the developing cortex in vivo, resulting in altered stratification of projection neurons and cortical layer malformation. Correct positioning of neurons in the mammalian cortex is a critical determinant of connectivity and neural function, as highlighted by severe neuronal migration disorders in humans (Ross and Walsh, 2001). Deficits in cortical patterning have also been suggested

in schizophrenia (Arnold, 1999). A recent study found high incidence of patches of neocortical disorganization in autistic brains (Stoner et al., 2014), reminiscent of what we observed in mouse cortex after in utero exploration to knockdown CYFIP1. Our study, therefore, provides a mechanistic model to understand how 15q11.2 CNVs as risk factors may contribute to susceptibility of neuropsychiatric disorders. Our study does not rule out the possibility that other factors within 15q11.2 CNVs affect neural development or that 15q11.2 CNVs also affect functional integrity of mature neurons, as suggested by rodent studies involving eIF4E (Napoli et al., 2008). Future studies of human neurons derived from our iPSC collection will help address the relevance of this pathway in human neuronal function.

Our study also reveals a critical role of the WAVE complex signaling in regulating neural stem cells. Early lethality of knockout mice for the majority of WAVE signaling components, including *CYFIP1* (Bozdagi et al., 2012), *WAVE2* (Yamazaki et al., 2003; Yan et al., 2003), *Abi1* (Dubielecka et al., 2011), and *Arp3* (Vauti et al., 2007), supports a requisite role of this pathway for mouse survival, which may have precluded in vivo investigation of its role in neural stem cells in early studies. Given that adherens junctions are rapidly lost in newly committed IPCs and neurons (Itoh et al., 2013; Rousso et al., 2012) and that there is little or reduced CYFIP1 expression in IPCs and immature neurons (Figure 3A), our result suggests that aberrant positioning of cortical projection neurons is caused by CYFIP1-WAVE signaling defects in RGCs. Future studies of cell-type-specific manipulation of CYFIP1-WAVE signaling in IPCs and/or immature neurons will provide a more definitive answer.

Human iPSC technology provides a new experimental platform to investigate cellular phenotypes and mechanisms in genetically tractable and disease-relevant human cell types. To date, patient-derived iPSCs, especially those related to monogenic disorders, have been successfully used to support models of disease pathology developed from animal studies, to demonstrate conserved cellular function of signaling pathways across species, or to facilitate large-scale screening of compounds to identify novel therapeutics (Bellin et al., 2012). Different from monogenic disorders, psychiatric disorders are often genetically complex and typically present with substantial variations in symptoms and degrees of impairment across individuals. Further, many risk-associated genetic mutations are not exclusive to clinical populations, nor a particular disease. A key challenge and opportunity for human iPSC biology is to generate new insight into (patho)physiological phenotypes and mechanisms beyond merely supporting previous findings and concepts. Using human iPSCs as a leading discovery tool, we identified consistent cellular phenotypes of neural stem cells that are specific for 15q11.2 del, as they were not present in hNPCs derived from iPSCs with a *DISC1* mutation, another risk factor for neuropsychiatric disorders (Thomson et al., 2013). While genetic risk factors for psychiatric disorders do not code for behavior, we provide an example that they can lead to specific cellular abnormalities of biological processes implicated in the neurodevelopmental origins of these disorders. Using human iPSCs as an entry point enabled identification of investigative targets, followed by validation of in vivo physiological relevance and identification of underlying mechanisms using animal models, and finally, a return to human genetic association studies to support the disease-relevance of the identified pathway in humans (Figure 1B).

In summary, by leveraging and integrating information derived from multiple levels of analyses, ranging from cellular processes in human neural stem cells, in vivo animal models, to targeted human genetic association studies, we provide a mechanistic understanding of how 15q11.2 microdeletion affects neural developmental processes. Furthermore, our study illustrates the potential of human iPSC-based research to enable a multifaceted approach to tackle the mystery of complex psychiatric disorders.

EXPERIMENTAL PROCEDURES

iPSC Generation, Culture, Characterization, and Neural Differentiation

All iPSC lines were derived from human donor dermal skin fibroblasts using integration-free episomal or Sendai virus methods. Fibroblasts with 15q11.2 del (Y1, Y3, and Y4) were collected through the National Institute of Mental Health (NIMH) childhood-onset schizophrenia cohort and their family members (Mattai et al., 2011). All procedures were performed in accordance with IRB and ISCRO protocols approved by the Institutional Committees. iPSCs were cultured and characterized as previously described (Chiang et al., 2011; Juopperi et al., 2012).

iPSCs were differentiated into pNPCs according to a published protocol (Li et al., 2011). Neural rosette formation assays were performed using the monolayer (Shi et al., 2012) and embryoid body methods (Juopperi et al., 2012). Neural rosettes were initially identified based on polarized pattern of DAPI staining and NESTIN immunoreactivity. Only individual nonoverlapped neural rosettes that were 50–200 μm in diameter were included for quantification. The number of rosettes showing an intact apical-ring structure (>90% of coverage of apical-ring circumference with atypical PKCλ, N-cadherin, PAR3, or β-catenin immunoreactivity) and incomplete/partial apical structure (<90% coverage) were quantified.

In Utero Electroporation and Quantitative Analysis of Mouse Cortical Development

In utero electroporation was performed as described (Saito, 2006). For quantitative analysis of electroporated neocortices, GFP^+ cells localized within the dorso-lateral cortex were examined. A total of three to six brain sections were analyzed per animal by taking 3 × 3 images to cover the electroporated region of each coronal section with a 25× or 40× objective and comparing them with equivalent sections in littermate counterparts. Quantifications were performed using Imaris software (Bitplane). For distribution plots, the distances between GFP^+Pax6^+ cells or GFP^+Tbr2^+ cells and the ventricular surface were calculated by using an in-house MATLAB script (MathWorks) and plotted after dividing each distance by total length of the neocortex and subgrouping into ten equal-size vertical bins (1: the most apical, 10: the most basal).

All animal procedures were performed in accordance with the protocol approved by the Institutional Animal Care and Use Committee.

mRNA Expression Analysis of Postmortem Human Brains, SNP Genotyping, and Clinical Genetic Association and Interaction Analyses

mRNA expression data were generated from postmortem DLPFC gray matter from 64 subjects without history or diagnosis of a medical or psychiatric disorder (51 males; mean age: 44 ± 14.9 years), all from European ancestry population and matched on age and various postmortem tissue characteristics. Detailed methods relating to the Brain Tissue Collection of the Clinical Brain Disorders Branch at NIMH (CBDB/NIMH) and the Lieber Institute for Brain Development (LIBD) have been described elsewhere (Colantuoni et al., 2011).

DNA for genotyping was obtained from the cerebella of samples in the collection using Illumina OMNI 2.5M SNP chips. We used ANCOVAs, with age, sex, and RIN (RNA integrity number) as covariates, to investigate main effects of SNPs on gene expression.

We carried out clinical genetic association and interaction analyses using logistic regression in four independent sample cohorts of cases with schizophrenia and healthy controls. Final interaction analysis was also assessed in the combined sample of four cohorts while controlling cohort effect in order to gain adequate power to detect interactions. The sample collection, genotyping, and quality control have been described elsewhere (Zhang et al., 2011).

SUPPLEMENTAL INFORMATION

Supplemental Information includes Supplemental Experimental Procedures, six figures, and six tables and can be found with this article online at http://dx.doi.org/10.1016/j.stem.2014.05.003.

ACKNOWLEDGMENTS

We would like to thank members of G.-l.M. and H.S. laboratories for discussion, ICE stem cell core and H. Kim for generating some iPSC lines, K. Ahn, T. Andersen, V. Villagomez, L. Liu, and Y. Cai for technical support and help. This work was supported by NIH (NS048271, HD069184), the Brain and Behavior Research Foundation (NARSAD), and the Maryland Stem Cell Research Fund (MSCRF) (to G.-l.M.), the Simons Foundation Autism Research Initiative (SFARI), NIH (NS047344, MH087874), and the International Mental Health Research Organization (IMHRO) to H.S., the Lieber Institute for Brain Development to D.R.W., J.E.K., and T.M.H., NARSAD and MSCRF to K.M.C., by fellowships from HFSP to K-j.Y. and MSCRF to G.M., N.-S.K., and Z.W., and from NIH (F31MH102978) to H.N.N.

Received: December 19, 2013
Revised: April 10, 2014
Accepted: May 12, 2014
Published: July 3, 2014

REFERENCES

Arnold, S.E. (1999). Neurodevelopmental abnormalities in schizophrenia: insights from neuropathology. Dev. Psychopathol. *11*, 439–456.

Bellin, M., Marchetto, M.C., Gage, F.H., and Mummery, C.L. (2012). Induced pluripotent stem cells: the new patient? Nat. Rev. Mol. Cell Biol. *13*, 713–726.

Bogdan, S., Grewe, O., Strunk, M., Mertens, A., and Klämbt, C. (2004). Sra-1 interacts with Kette and Wasp and is required for neuronal and bristle development in Drosophila. Development *131*, 3981–3989.

Bozdagi, O., Sakurai, T., Dorr, N., Pilorge, M., Takahashi, N., and Buxbaum, J.D. (2012). Haploinsufficiency of Cyfip1 produces fragile X-like phenotypes in mice. PLoS ONE *7*, e42422.

Buchman, J.J., and Tsai, L.H. (2007). Spindle regulation in neural precursors of flies and mammals. Nat. Rev. Neurosci. *8*, 89–100.

Chiang, C.H., Su, Y., Wen, Z., Yoritomo, N., Ross, C.A., Margolis, R.L., Song, H., and Ming, G.L. (2011). Integration-free induced pluripotent stem cells derived from schizophrenia patients with a DISC1 mutation. Mol. Psychiatry *16*, 358–360.

Christian, K., Song, H., and Ming, G. (2012). Application of reprogrammed patient cells to investigate the etiology of neurological and psychiatric disorders. Front. Biol. *7*, 179–188.

Colantuoni, C., Lipska, B.K., Ye, T., Hyde, T.M., Tao, R., Leek, J.T., Colantuoni, E.A., Elkahloun, A.G., Herman, M.M., Weinberger, D.R., and Kleinman, J.E. (2011). Temporal dynamics and genetic control of transcription in the human prefrontal cortex. Nature *478*, 519–523.

Cooper, G.M., Coe, B.P., Girirajan, S., Rosenfeld, J.A., Vu, T.H., Baker, C., Williams, C., Stalker, H., Hamid, R., Hannig, V., et al. (2011). A copy number variation morbidity map of developmental delay. Nat. Genet. *43*, 838–846.

de Kovel, C.G., Trucks, H., Helbig, I., Mefford, H.C., Baker, C., Leu, C., Kluck, C., Muhle, H., von Spiczak, S., Ostertag, P., et al. (2010). Recurrent microdeletions at 15q11.2 and 16p13.11 predispose to idiopathic generalized epilepsies. Brain *133*, 23–32.

De Wolf, V., Brison, N., Devriendt, K., and Peeters, H. (2013). Genetic counseling for susceptibility loci and neurodevelopmental disorders: the del15q11.2 as an example. Am. J. Med. Genet. A. *161A*, 2846–2854.

Dubielecka, P.M., Ladwein, K.I., Xiong, X., Migeotte, I., Chorzalska, A., Anderson, K.V., Sawicki, J.A., Rottner, K., Stradal, T.E., and Kotula, L. (2011). Essential role for Abi1 in embryonic survival and WAVE2 complex integrity. Proc. Natl. Acad. Sci. USA *108*, 7022–7027.

Englund, C., Fink, A., Lau, C., Pham, D., Daza, R.A., Bulfone, A., Kowalczyk, T., and Hevner, R.F. (2005). Pax6, Tbr2, and Tbr1 are expressed sequentially by radial glia, intermediate progenitor cells, and postmitotic neurons in developing neocortex. J. Neurosci. *25*, 247–251.

Galy, A., Schenck, A., Sahin, H.B., Qurashi, A., Sahel, J.A., Diebold, C., and Giangrande, A. (2011). CYFIP dependent actin remodeling controls specific aspects of Drosophila eye morphogenesis. Dev. Biol. *359*, 37–46.

Geschwind, D.H. (2009). Advances in autism. Annu. Rev. Med. *60*, 367–380.

International Schizophrenia Consortium (2008). Rare chromosomal deletions and duplications increase risk of schizophrenia. Nature *455*, 237–241.

Itoh, Y., Moriyama, Y., Hasegawa, T., Endo, T.A., Toyoda, T., and Gotoh, Y. (2013). Scratch regulates neuronal migration onset via an epithelial-mesenchymal transition-like mechanism. Nat. Neurosci. *16*, 416–425.

Jähn, J.A., von Spiczak, S., Muhle, H., Obermeier, T., Franke, A., Mefford, H.C., Stephani, U., and Helbig, I. (2014). Iterative phenotyping of 15q11.2, 15q13.3 and 16p13.11 microdeletion carriers in pediatric epilepsies. Epilepsy Res. *108*, 109–116.

Juopperi, T.A., Kim, W.R., Chiang, C.H., Yu, H., Margolis, R.L., Ross, C.A., Ming, G.L., and Song, H. (2012). Astrocytes generated from patient induced pluripotent stem cells recapitulate features of Huntington's disease patient cells. Mol. Brain *5*, 17.

Kirov, G., Grozeva, D., Norton, N., Ivanov, D., Mantripragada, K.K., Holmans, P., Craddock, N., Owen, M.J., and O'Donovan, M.C.; International Schizophrenia Consortium; Wellcome Trust Case Control Consortium (2009). Support for the involvement of large copy number variants in the pathogenesis of schizophrenia. Hum. Mol. Genet. *18*, 1497–1503.

Kobayashi, K., Kuroda, S., Fukata, M., Nakamura, T., Nagase, T., Nomura, N., Matsuura, Y., Yoshida-Kubomura, N., Iwamatsu, A., and Kaibuchi, K. (1998). p140Sra-1 (specifically Rac1-associated protein) is a novel specific target for Rac1 small GTPase. J. Biol. Chem. *273*, 291–295.

Kriegstein, A., and Alvarez-Buylla, A. (2009). The glial nature of embryonic and adult neural stem cells. Annu. Rev. Neurosci. *32*, 149–184.

Kunda, P., Craig, G., Dominguez, V., and Baum, B. (2003). Abi, Sra1, and Kette control the stability and localization of SCAR/WAVE to regulate the formation of actin-based protrusions. Curr. Biol. *13*, 1867–1875.

Leone, D.P., Srinivasan, K., Chen, B., Alcamo, E., and McConnell, S.K. (2008). The determination of projection neuron identity in the developing cerebral cortex. Curr. Opin. Neurobiol. *18*, 28–35.

Li, W., Sun, W., Zhang, Y., Wei, W., Ambasudhan, R., Xia, P., Talantova, M., Lin, T., Kim, J., Wang, X., et al. (2011). Rapid induction and long-term self-renewal of primitive neural precursors from human embryonic stem cells by small molecule inhibitors. Proc. Natl. Acad. Sci. USA *108*, 8299–8304.

Loulier, K., Lathia, J.D., Marthiens, V., Relucio, J., Mughal, M.R., Tang, S.C., Coksaygan, T., Hall, P.E., Chigurupati, S., Patton, B., et al. (2009). beta1 integrin maintains integrity of the embryonic neocortical stem cell niche. PLoS Biol. *7*, e1000176.

Malhotra, D., and Sebat, J. (2012). CNVs: harbingers of a rare variant revolution in psychiatric genetics. Cell *148*, 1223–1241.

Mattai, A.A., Weisinger, B., Greenstein, D., Stidd, R., Clasen, L., Miller, R., Tossell, J.W., Rapoport, J.L., and Gogtay, N. (2011). Normalization of cortical gray matter deficits in nonpsychotic siblings of patients with childhood-onset schizophrenia. J. Am. Acad. Child Adolesc. Psychiatry *50*, 697–704.

Mullen, S.A., Carvill, G.L., Bellows, S., Bayly, M.A., Trucks, H., Lal, D., Sander, T., Berkovic, S.F., Dibbens, L.M., Scheffer, I.E., and Mefford, H.C. (2013). Copy number variants are frequent in genetic generalized epilepsy with intellectual disability. Neurology *81*, 1507–1514.

Napoli, I., Mercaldo, V., Boyl, P.P., Eleuteri, B., Zalfa, F., De Rubeis, S., Di Marino, D., Mohr, E., Massimi, M., Falconi, M., et al. (2008). The fragile X syndrome protein represses activity-dependent translation through CYFIP1, a new 4E-BP. Cell *134*, 1042–1054.

Nishimura, Y., Martin, C.L., Vazquez-Lopez, A., Spence, S.J., Alvarez-Retuerto, A.I., Sigman, M., Steindler, C., Pellegrini, S., Schanen, N.C., Warren, S.T., and Geschwind, D.H. (2007). Genome-wide expression profiling of lymphoblastoid cell lines distinguishes different forms of autism and reveals shared pathways. Hum. Mol. Genet. *16*, 1682–1698.

Rasin, M.R., Gazula, V.R., Breunig, J.J., Kwan, K.Y., Johnson, M.B., Liu-Chen, S., Li, H.S., Jan, L.Y., Jan, Y.N., Rakic, P., and Sestan, N. (2007). Numb and Numbl are required for maintenance of cadherin-based adhesion and polarity of neural progenitors. Nat. Neurosci. *10*, 819–827.

Ross, M.E., and Walsh, C.A. (2001). Human brain malformations and their lessons for neuronal migration. Annu. Rev. Neurosci. *24*, 1041–1070.

Rousso, D.L., Pearson, C.A., Gaber, Z.B., Miquelajauregui, A., Li, S., Portera-Cailliau, C., Morrisey, E.E., and Novitch, B.G. (2012). Foxp-mediated suppression of N-cadherin regulates neuroepithelial character and progenitor maintenance in the CNS. Neuron *74*, 314–330.

Saito, T. (2006). In vivo electroporation in the embryonic mouse central nervous system. Nat. Protoc. *1*, 1552–1558.

Schenck, A., Bardoni, B., Moro, A., Bagni, C., and Mandel, J.L. (2001). A highly conserved protein family interacting with the fragile X mental retardation protein (FMRP) and displaying selective interactions with FMRP-related proteins FXR1P and FXR2P. Proc. Natl. Acad. Sci. USA *98*, 8844–8849.

Schenck, A., Bardoni, B., Langmann, C., Harden, N., Mandel, J.L., and Giangrande, A. (2003). CYFIP/Sra-1 controls neuronal connectivity in Drosophila and links the Rac1 GTPase pathway to the fragile X protein. Neuron *38*, 887–898.

Shi, Y., Kirwan, P., Smith, J., Robinson, H.P.C., and Livesey, F.J. (2012). Human cerebral cortex development from pluripotent stem cells to functional excitatory synapses. Nat. Neurosci. *15*, 477–486.

Stefansson, H., Rujescu, D., Cichon, S., Pietiläinen, O.P., Ingason, A., Steinberg, S., Fossdal, R., Sigurdsson, E., Sigmundsson, T., Buizer-Voskamp, J.E., et al.; GROUP (2008). Large recurrent microdeletions associated with schizophrenia. Nature *455*, 232–236.

Stefansson, H., Meyer-Lindenberg, A., Steinberg, S., Magnusdottir, B.B., Morgen, K., Arnarsdottir, S., and Stefansson, K. (2014). CNVs conferring risk of autism or schizophrenia affect cognition in controls. Nature *505*, 361–366.

Steffen, A., Rottner, K., Ehinger, J., Innocenti, M., Scita, G., Wehland, J., and Stradal, T.E. (2004). Sra-1 and Nap1 link Rac to actin assembly driving lamellipodia formation. EMBO J. *23*, 749–759.

Stoner, R., Chow, M.L., Boyle, M.P., Sunkin, S.M., Mouton, P.R., Roy, S., Wynshaw-Boris, A., Colamarino, S.A., Lein, E.S., and Courchesne, E. (2014). Patches of disorganization in the neocortex of children with autism. N. Engl. J. Med. *370*, 1209–1219.

Tam, G.W., van de Lagemaat, L.N., Redon, R., Strathdee, K.E., Croning, M.D., Malloy, M.P., Muir, W.J., Pickard, B.S., Deary, I.J., Blackwood, D.H., et al. (2010). Confirmed rare copy number variants implicate novel genes in schizophrenia. Biochem. Soc. Trans. *38*, 445–451.

Thomson, P.A., Malavasi, E.L., Grünewald, E., Soares, D.C., Borkowska, M., and Millar, J.K. (2013). DISC1 genetics, biology and psychiatric illness. Front. Biol. (Beijing) *8*, 1–31.

van der Zwaag, B., Staal, W.G., Hochstenbach, R., Poot, M., Spierenburg, H.A., de Jonge, M.V., Verbeek, N.E., van 't Slot, R., van Es, M.A., Staal, F.J., et al. (2010). A co-segregating microduplication of chromosome 15q11.2 pinpoints two risk genes for autism spectrum disorder. Am. J. Med. Genet. B. Neuropsychiatr. Genet. *153B*, 960–966.

Vauti, F., Prochnow, B.R., Freese, E., Ramasamy, S.K., Ruiz, P., and Arnold, H.H. (2007). Arp3 is required during preimplantation development of the mouse embryo. FEBS Lett. *581*, 5691–5697.

Wegiel, J., Frackowiak, J., Mazur-Kolecka, B., Schanen, N.C., Cook, E.H., Jr., Sigman, M., Brown, W.T., Kuchna, I., Wegiel, J., Nowicki, K., et al. (2012). Abnormal intracellular accumulation and extracellular Aβ deposition in idiopathic and Dup15q11.2-q13 autism spectrum disorders. PLoS ONE *7*, e35414.

Weinberger, D.R. (1987). Implications of normal brain development for the pathogenesis of schizophrenia. Arch. Gen. Psychiatry *44*, 660–669.

Yamazaki, D., Suetsugu, S., Miki, H., Kataoka, Y., Nishikawa, S., Fujiwara, T., Yoshida, N., and Takenawa, T. (2003). WAVE2 is required for directed cell migration and cardiovascular development. Nature *424*, 452–456.

Yan, C., Martinez-Quiles, N., Eden, S., Shibata, T., Takeshima, F., Shinkura, R., Fujiwara, Y., Bronson, R., Snapper, S.B., Kirschner, M.W., et al. (2003). WAVE2 deficiency reveals distinct roles in embryogenesis and Rac-mediated actin-based motility. EMBO J. *22*, 3602–3612.

Zhang, F., Chen, Q., Ye, T., Lipska, B.K., Straub, R.E., Vakkalanka, R., Rujescu, D., St. Clair, D., Hyde, T.M., Bigelow, L., et al. (2011). Evidence of sex-modulated association of ZNF804A with schizophrenia. Biol. Psychiatry *69*, 914–917.

Zhao, L., Wang, D., Wang, Q., Rodal, A.A., and Zhang, Y.Q. (2013a). Drosophila CYFIP regulates synaptic development and endocytosis by suppressing filamentous actin assembly. PLoS Genet. *9*, e1003450.

Zhao, Q., Li, T., Zhao, X., Huang, K., Wang, T., Li, Z., Ji, J., Zeng, Z., Zhang, Z., Li, K., et al. (2013b). Rare CNVs and tag SNPs at 15q11.2 are associated with schizophrenia in the Han Chinese population. Schizophr. Bull. *39*, 712–719.

Cell Stem Cell, Volume *15*

Supplemental Information

Modeling a Genetic Risk for Schizophrenia in iPSCs and Mice Reveals Neural Stem Cell Deficits Associated with Adherens Junctions and Polarity

Ki-Jun Yoon, Ha Nam Nguyen, Gianluca Ursini, Fengyu Zhang, Nam-Shik Kim, Zhexing Wen, Georgia Makri, David Nauen, Joo Heon Shin, Youngbin Park, Raeeun Chung, Eva Pekle, Ce Zhang, Maxwell Towe, Syed Mohammed Qasim Hussaini, Yohan Lee, Dan Rujescu, David St. Clair, Joel E. Kleinman, Thomas M. Hyde, Gregory Krauss, Kimberly M. Christian, Judith L. Rapoport, Daniel R. Weinberger, Hongjun Song, and Guo-li Ming

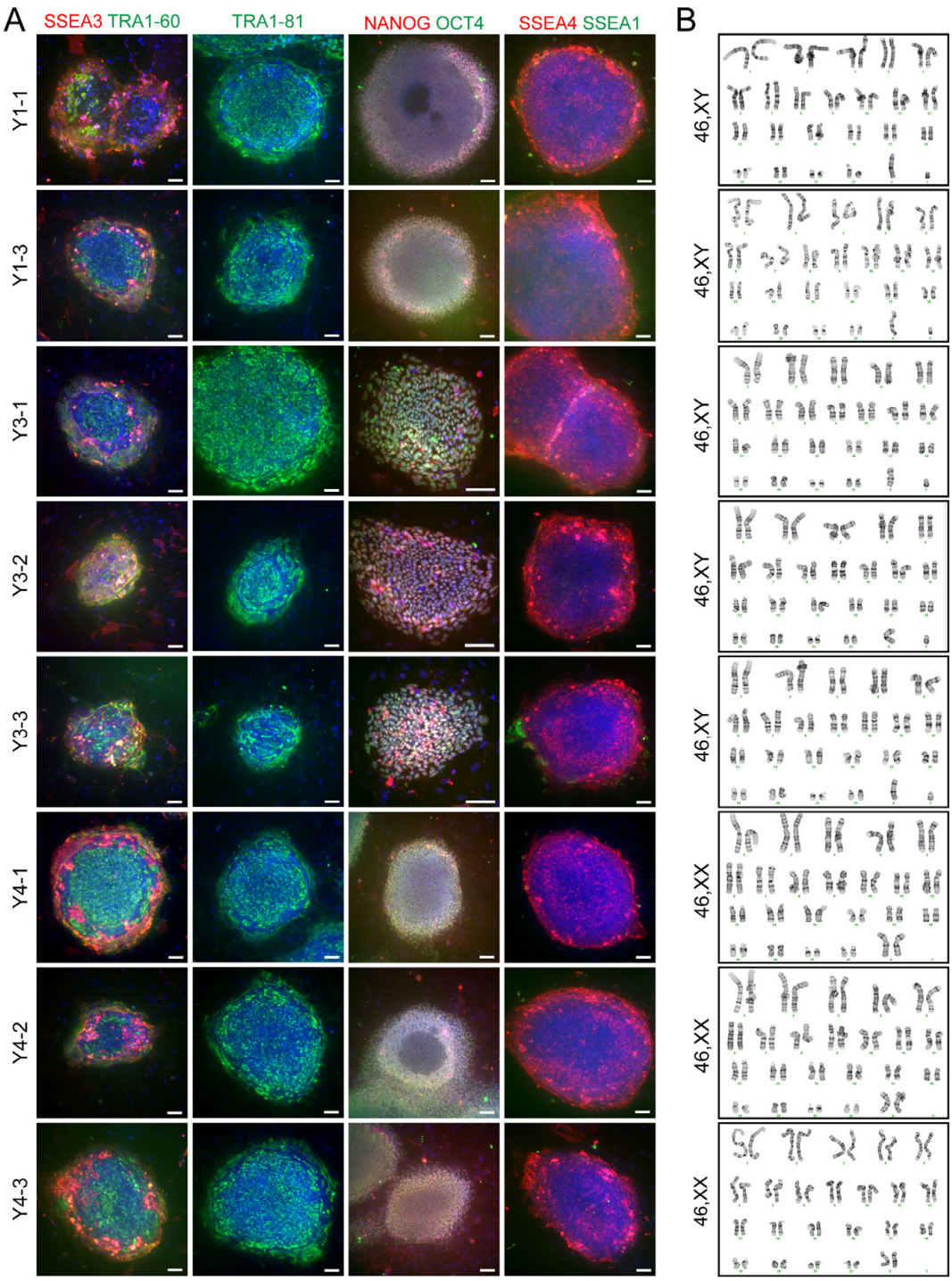

Figure S1. Characterization of iPSC lines with or without 15q11.2del, related to Figure 1
(A) Sample images of immunostaining of different iPSC lines. Note that all iPSC lines were positive for pluripotency markers, including SSEA3, TRA1-60, TRA1-81, NANOG, OCT4, and SSEA4, and were negative for SSEA1. Scale bars: 100 μm.
(B) Sample images of normal karyotypes analyzed by G-banding for the same iPSC lines shown in (A).

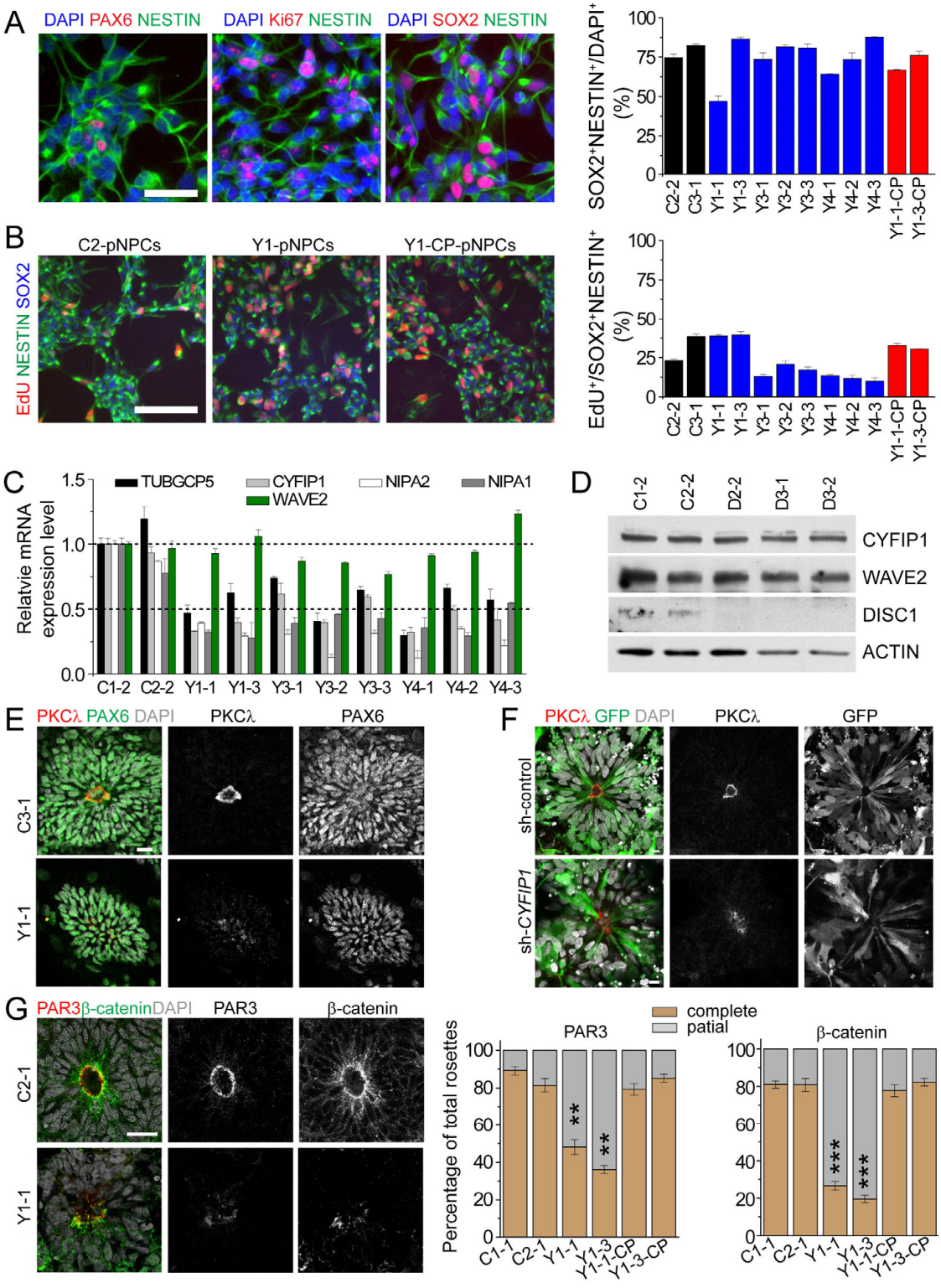

Figure S2. Characterization of hNPCs differentiated from iPSC lines with or without 15q11.2del, related to Figures 1 and 2

(A) Normal differentiation of iPSCs with 15q11.2del into primitive NPCs (pNPCs). Shown on the left are sample images of immunostaining for NESTIN, PAX6, SOX2 and Ki67. Scale bar, 50 μm. Shown on the right is a summary of quantifications of percentages of $SOX2^{+}NESTIN^{+}$ pNPCs among all $DAPI^{+}$ cells. Values represent mean ± SEM (n = 3 cultures).

(B) Proliferation of pNPCs derived from different iPSC lines. Cultures were pulsed with EdU (20 μM) for 4 hrs before analysis. Shown on the left are sample images of staining for NESTIN, SOX2 and EdU. Scale bar, 100 μm. Shown on the right is a summary of percentages of EdU^+ cells among all $SOX2^+NESTIN^+$ cells. Values represent mean ± SEM (n = 3 cultures).
(C) mRNA levels of four genes within the 15q11.2 microdeletion and WAVE2 in pNPCs derived from different iPSC lines. Values represent mean ± SEM (n = 3 cultures).
(D) Sample Western blot images of pNPCs from different iPSC lines.
(E) Sample confocal images of immunostaining of PKCλ and PAX6 for neural rosettes generated using the embryoid body method.
(F) Sample confocal images of immunostaining of PKCλ for neural rosettes after CYFIP1 knockdown. Scale bars, 10 μm. Neural rosettes from C3-1 iPSCs were infected with lentiviruses to co-express GFP and sh-*CYFIP1* and examined 3 days later.
(G) Defects in adherens junctions and apical polarity of hNPCs derived from iPSCs with 15q11.2 microdeletion as shown by PAR3 and β-catenin immunostaining. Shown on the left are sample confocal images of immunostaining of atypical PAR3 and β-catenin for neural rosettes differentiated from iPSCs by the embryoid body method. Scale bar, 20 μm. Shown on the right are quantifications of neural rosettes with complete “apical ring-like structure” (≥ 90% coverage of apical-ring circumference with PAR3 or β-catenin immunoreactivity) or “partial/scattered” (< 90% coverage). Values represent mean ± SEM (n = 3 cultures; $^{**}p < 0.01$; $^{***}p < 0.001$; Student’s t-test).

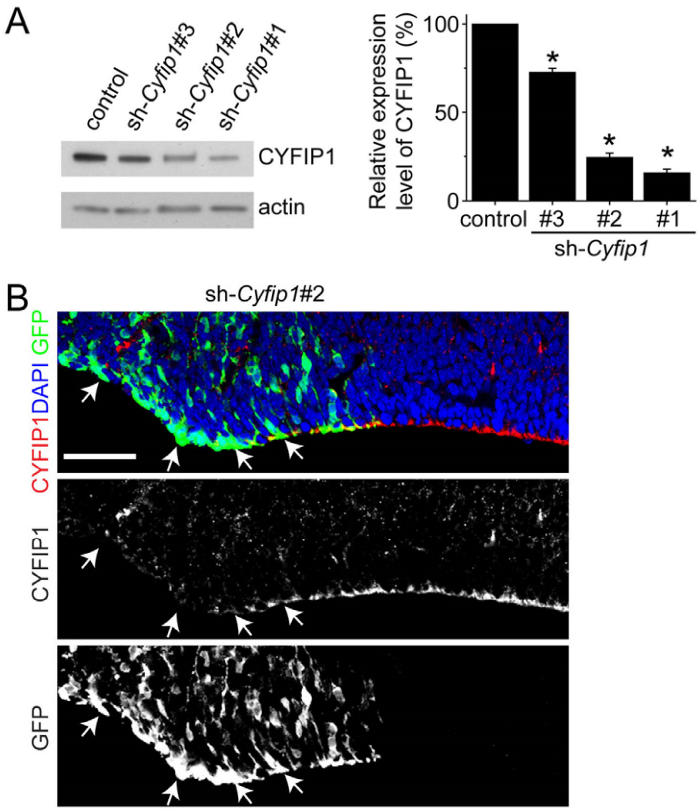

Figure S3. Characterization of shRNAs against mouse *Cyfip1*, related to Figure 3
(A) Efficacy of different shRNAs against mouse *Cyfip1*. Mouse NPCs were infected with retroviruses to express one of the three shRNAs against mouse *Cyfip1* and examined 3 days later. Shown on the left are sample Western blot images and on the right is a summary of quantification. Values represent mean ± SEM (n = 3 cultures; *p < 0.05; Student's t-test).
(B) Effective knockdown of CYFIP1 protein expression by sh-*Cyfip1*#2. E13.5 embryos were electroporated to co-express GFP and sh-*Cyfip1*#2 and examined at E16.5. Shown are sample confocal images of immunostaining for GFP, CYFIP1 and DAPI. Scale bar, 50 μm.

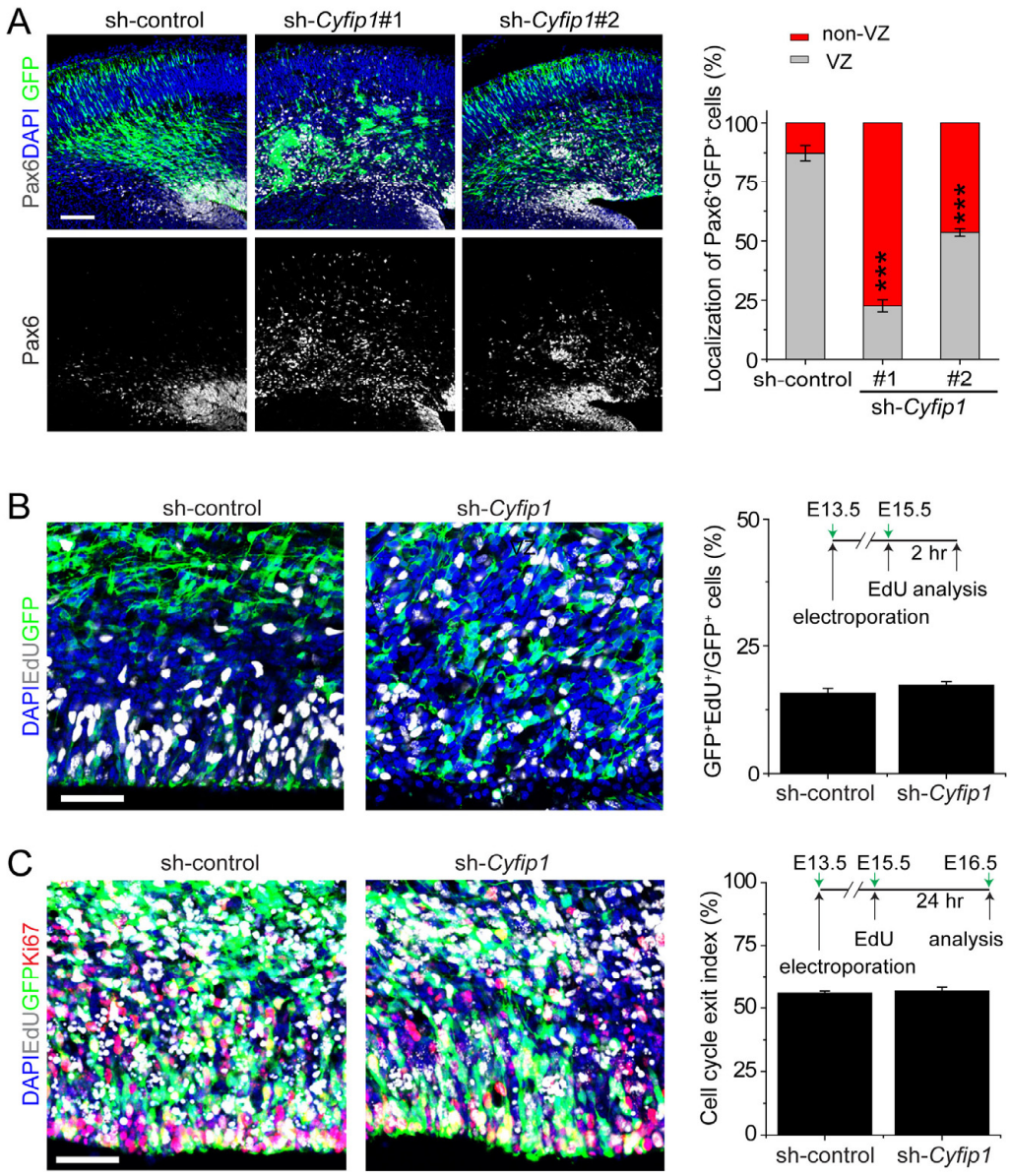

Figure S4. Normal proliferation and cell cycle exit of CYFIP1-deficient NPCs in the developing mouse cortex, related to Figure 4

(A) Ectopic localization of Pax6$^+$ RGCs outside of the VZ after in utero electroporation of two different shRNAs against mouse *Cyfip1*. Same as in Figures 4A-B, except that sh-control, sh-*Cyfip1*#1 and *Cyfip1*#2 were examined. Scale bar: 50 μm.

(B) Normal proliferation of CYFIP1-deficent NPCs in the developing cortex. E13.5 embryos were electroporated to co-express GFP and sh-control or sh-*Cyfip1*. EdU (50 mg/kg body weight) was injected at E15.5 for analyses 2 hrs later. Shown on the left are sample confocal images of staining for GFP, EdU and DAPI. Scale bar: 50 μm. Shown on the right is a summary of percentages of EdU$^+$ cells among all GFP$^+$ cells. Values represent mean ± SEM (n = 4 animals).

(C) Normal cell cycle exit of CYFIP1-deficent NPCs. Same as in (B), except that analyses were performed at E16.5. Shown on the left are sample confocal images of staining for GFP, Ki67, EdU and DAPI. Scale bar: 50 μm. Shown on the right is a summary of cell cycle exit index, which is defined as percentages of GFP$^+$EdU$^+$Ki67$^-$ cells among total GFP$^+$EdU$^+$ cells. Values represent mean ± SEM (n = 4 animals).

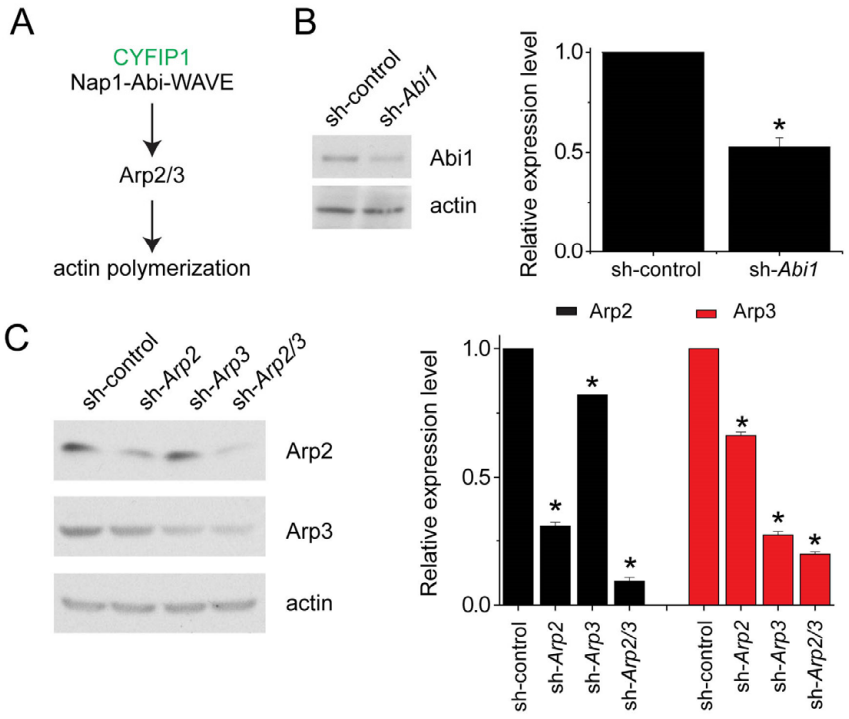

Figure S5. Characterization of shRNAs against mouse WAVE signalling components, related to Figure 6

(A) A schematic diagram of CYFIP1-WAVE complex signalling.

(B) Effective shRNA against mouse *Abi1*. Mouse NPCs were infected with retroviruses to express a specific shRNA against mouse *Abi1* and examined 3 days later. Shown are sample Western blot images (left) and summary of quantification (right). Values represent mean ± SEM (n = 3 cultures; *p < 0.05; Student's t-test).

(C) Effective shRNAs against mouse *Arp2 and Arp3.* Same as in (B), except that mouse NPCs were infected with retroviruses to express shRNA against mouse *Arp2* or *Arp3*, or co-infected with two retroviruses for double knockdown. Values represent mean ± SEM (n = 3 cultures; *p < 0.05; Student's t-test)

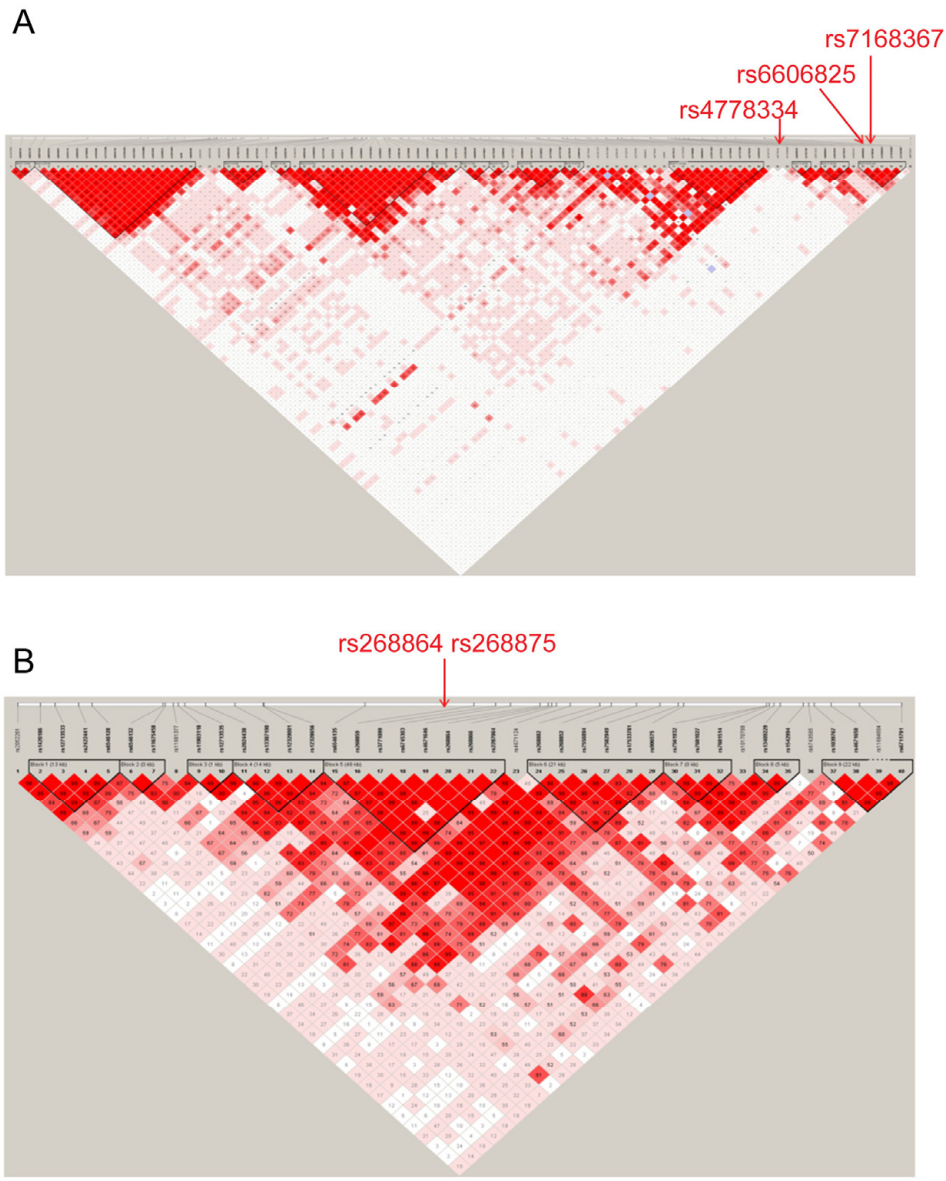

Figure S6. Linkage disequilibrium plots of two genes *CYFIP1* and *ACRT2* showing significant interaction, related to Figure 7

(A) Linkage disequilibrium (R-squared measure) of SNPs in *CYFIP1* (HapMap CEU data) showing three SNPs that were used for the interaction analysis.

(B) Linkage disequilibrium (R-squared measure) of SNPs in *ACTR2* (HapMaP CEU data) showing two SNPs that were used for the interaction analysis.

Table S1. iPSC characterization, related to Figures 1 and 2

iPSC lines clones #	Genotype	DNA FISH Confirmation (CYFIP1 Del.)	Karyotype	Pluripotency (TRA160/81+, SSEA4/3+)	Teratoma	Sex/Age
C1-1	Wild type	Yes	Normal	Yes	Yes	M/Fetal
C1-2	Wild type	Yes	Normal	Yes	Yes	M/Fetal
C2-1	Wild type	Yes	Normal	Yes	Yes	F/70
C2-2	Wild type	Yes	Normal	Yes	Yes	F/70
C3-1	Wild type	Yes	Normal	Yes	Yes	F/40
C3-2	Wild type	Yes	Normal	Yes	Yes	F/40
Y1-1	15q11.2 del	Yes	Normal	Yes	Yes	M/52.8
Y1-3	15q11.2 del	Yes	Normal	Yes	Yes	M/52.8
Y3-1	15q11.2 del	Yes	Normal	Yes	nd	M/14.8
Y3-2	15q11.2 del	Yes	Normal	Yes	Yes	M/14.8
Y3-3	15q11.2 del	Yes	Normal	Yes	nd	M/14.8
Y4-1	15q11.2 del	Yes	Normal	Yes	Yes	F/46.4
Y4-2	15q11.2 del	Yes	Normal	Yes	Yes	F/46.4
Y4-3	15q11.2 del	Yes	Normal	Yes	Yes	F/46.4
Y1-1-CP	15q11.2 del	nd	Normal	Yes	nd	M/52.8
Y1-3-CP	15q11.2 del	nd	Normal	Yes	nd	M/52.8
D2-1	DISC1 4bp deletion	Yes	Normal	Yes	Yes	F/40
D2-2	DISC1 4bp deletion	Yes	Normal	Yes	Yes	F/40
D3-1	DISC1 4bp deletion	Yes	Normal	Yes	Yes	M/70
D3-2	DISC1 4bp deletion	Yes	Normal	Yes	Yes	M/70

Table S2. Antibody information, related to Figures 1, 2, 3, 4, 5, and 6

Antibodies	Host species	Companies	Catalog Number	Wetern blotting	Immunofluorescence
Atypical PKCλ	Mouse	BD Transduction Laboratory	610207		1/500
N-cadherin	Mouse	Invitrogen	18-0224		1/500
Pax6	Rabbit	Covance	PRB-278P		1/1000
PAR3	Rabbit	Milipore	07-330		1/500
CYFIP1	Rabbit	Milipore	AB6046	1/3000	1/1000
CTIP2	Rat	Abcam	AB18465		1/200
Cux1	Rabbit	Santacruz Biotechnology	sc-13024		1/1000
Nestin	Chichen	Aves Labs	Nes		1/2000 (for mouse)
Nestin	Rabbit	Millipore	AB5922	1/2000	1/1000 (for human)
DISC1	Rabbit	Kozo Kaibuchi lab		1/1000	
Nckap1, Nap1	Rabbit	Abcam	AB96715	1/1000	
WAVE1	Goat	Santacruz Biotechnology	sc-10388	1/2000	
WAVE2	Rabbit	Santacruz Biotechnology	sc-33548	1/1000	1/500
Actin	Mouse	Milipore	MAB1501	1/10000	
Abi1	Mouse	MBL	D147-3	1/1000	
Arp2	Mouse	Abcam	ab49674	1/1000	
Arp3	Mouse	Abcam	ab56817	1/1000	
β-catenin	Mouse	BD Transduction Laboratory	610153		1/1000
HA	Mouse	Covance	MMS-101P		1/500
GFP	sheep	AbD SeroTec	4745-1051		1/1000
Tbr2	Rabbit	Abcam	ab23345		1/1000
Ki-67	Rabbit	Leica Microsystems	NCL-Ki67p		1/400
OCT3/4	Mouse	Santacruz Biotechnology	sc-365509		1/400
NANOG	Goat	R & D Systems	AF1997		1/200
SSEA3	Rat	Millipore	MAB4303		1/500
SSEA4	Mouse	Millipore	MAB4304		1/500
SSEA1	Mouse	Millipore	MAB4301		1/500
TRA1-60	Mouse	Millipore	MAB4360		1/500
TRA1-81	Mouse	Millipore	MAB4381		1/500

Table S3. shRNA sequences used in the current study, related to Figures 2, 3, and 6.

Species	shRNA	Sequence	Reference
mouse	non-target control	5'-TTCTCCGAACGTGTCACGT-3'	Qiagen
mouse	*Cyfip1*#1	5'-GAATTACCCTCCACGTCTTCTGGG-3'	Silva et al.,2009
mouse	*Cyfip1*#2	5'-GCATGTTTGTCTTTATGTA-3'	
mouse	*Abi1*	5'-CTCGAAGAGAGATTGGTAT-3'	Sun et al.,2008
mouse	*Arp2*	5'-TGACCATGGCTTTAAACAA-3'	Wu et al.,2012
mouse	*Arp3*	5'-TCGCCATGGTATAGTTGAA-3'	
human	*hCYFIP1*	5'-GCAAAGATGAGATTATTAA-3'	Silva et al.,2009

Table S4. SNPs significantly associated with gene expression determined using RNA sequencing in human post-mortem brains of normal subjects based on analysis of covariance, controlling for age, sex and RIN, related to Figure 7.

SNP	Chr	Gene	rs	Position (hg19)	F	p	Sig
1	2	*ACTR2*	rs268864/rs268875[1]	65495887	5.64	0.02	*
2	10	*ABI1//C10orf51*	rs2797930	27210569	5.85	0.02	*
3	15	*CYFIP1//NIPA2*	rs4778334[2]	23040856	3.8	0.05	*
4	15	*CYFIP1//NIPA1*	rs6606825/rs7168367[3]	23062802	6.33	0.006	**

[1] SNPs in LD (D'= 1, r-square=0.831) according to HapMap CEU data (see Figure S6B);
[2] SNP with recent evidence of association with schizophrenia in Han Chinese population (Zhao et al., 2013);
[3] SNPs in LD (D'=1, r-square=0/99) (see Figure S6A).
*: $p < 0.05$; **$p < 0.01$

Table S5. Summary statistics and pair-wise correlation coefficient of expressions of the WAVE signaling, genes in postmortem human brains of normal subjects (n = 64), controlling for RIN (Highlighted cells indicate $p < 0.05$), related to Figure 7.

	Summary			Regression coefficient						
	Mean	SD	Median	*CYFIP1*	*WASF2*	*ABI1*	*WASF1*	*NCKAP1*	*ACTR2*	*ACTR3*
Control										
CYFIP1	3.78	0.75	3.76	1	-0.281	0.789	0.913	-0.258	-0.518	-1.676
WASF2	3.32	1.53	2.99	-0.281	1	-3.152	-5.827	-4.124	-3.215	-2.789
ABI1	8.91	1.88	9.05	0.789	-3.152	1	5.695	8.166	5.426	5.806
WASF1	34.88	8.94	37.01	0.913	-5.827	5.695	1	7.554	7.327	5.764
NCKAP1	35.65	11.54	38.49	-0.258	-4.124	8.166	7.554	1	10.932	10.931
ACTR2	44.81	11.95	47.16	-0.518	-3.215	5.426	7.327	10.932	1	10.945
ACTR3	17.03	3.67	17.41	-1.676	-2.789	5.806	5.764	10.931	10.945	1

Table S6. Single SNP association analysis of brain gene expression-associated SNPs in four cohorts of schizophrenia cases and controls in European ancestry population, related to Figure 7.

				LIBD/CBDB						GRU		ABE		MUN	
SNP	Chr	Gene	Rs no.	A1	F_A	F_U	A2	OR	p	OR	p	OR	P	OR	p
1	2	*ACTR2*	rs268864	G	0.148	0.149	A	0.987	0.900	0.993	0.931	1.115	0.329	1.192	0.162
2	10	*ABI1//C10orf51*	rs2797930	G	0.089	0.083	A	1.072	0.599	1.014	0.902	NA	NA	NA	NA
3	15	*CYFIP1//NIPA2*	rs4778334	T	0.262	0.231	C	1.182	0.050	1.042	0.571	0.978	0.824	0.936	0.523
4	15	*CYFIP1//NIPA1*	rs7168367	T	0.126	0.139	C	0.896	0.327	0.958	0.595	1.022	0.867	0.926	0.556

Note:
A1, A2 are nucleotides of major and minor allele;
F_A and F_U, minor allele frequency in cases with schizophrenia and controls;
OR, odds ratio measuring the strength and direction of minor allele with schizophrenia status.

Supplemental Experimental Procedures

iPSC Generation, Culture and Characterization

All iPSC lines were derived from human donor dermal skin fibroblasts using integration-free episomal or Sendai virus methods. iPSC lines (C1 and D2) were previously characterized (Chiang et al., 2011). Fibroblasts with 15q11.2 microdeletion (Y1, Y3, and Y4) were collected through the NIMH childhood-onset schizophrenia cohort and their family members (Mattai et al., 2011). All procedures were performed in accordance with the IRB and ISCRO protocols approved by the Institutional Committees.

iPSCs were cultured as previously described (Chiang et al., 2011; Juopperi et al., 2012). Briefly, they were plated on mouse embryonic fibroblast (MEF) feeders in standard human embryonic stem cell medium containing DMEM:F12 (Invitrogen), 20% Knock-out serum replacement (Invitrogen), 2-Mercaptoethanol (Millipore), Non-essential amino acids (Invitrogen), Pen/Strep (Invitrogen) and 10 ng/ml bFGF (Peprotech), and incubated at 37ºC and 5% CO_2. iPSCs were passaged every 5-7 days using 1 mg/ml Collagenase Type IV (Invitrogen).

Karyotyping analysis by standard G-banding technique was carried out by the Cytogenetics Core Facility at the Johns Hopkins Hospital or Cell Line Genetics Inc. Results were interpreted by clinical laboratory specialists of the Cytogenetics Core.

Teratoma formation assay was performed as previously described (Chiang et al., 2011). Briefly, iPSCs from a confluent 10-cm dish were harvested by Collagenase IV treatment and injected subcutaneously into female SCID mice (BL17SCID, Charles River). After 5-8 weeks post-transplantation, tumors were dissected from the host, fixed in 4% paraformaldehyde/PBS solution, paraffin embedded, sectioned and stained with Hematoxylin and Eosin.

DNA Fluorescence in Situ Hybridization

iPSCs were treated with KaryoMAX Colcemid solution (0.02 μg/ml, Invitrogen) overnight and dissociated with Accutase. Metaphase spread preparation and pre-treatment of cells for DNA FISH was followed as previously described (Nguyen and Reijo Pera, 2008). Both interphase nuclei and metaphase spreads were probed with SureFISH 15q11.2 *SNRPN* (G100006R, Agilent Technologies) and SureFISH 15q11.2 *CYFIP1* (G100543G, Agilent Technologies), and counter-stained with DAPI.

Neural Differentiation and Rosette Formation of Human iPSCs

iPSCs were differentiated into primitive neural precursor cells (pNPCs) according to a previously published protocol (Li et al., 2011). Briefly, iPSCs were passaged onto MEF feeders, and after three days, induction medium containing Advanced DMEM:F12 (50%) and Neurobasal medium (50%), CHIR99201 (4 μg/ml, Cellagentech), SB431542 (3 μg/ml, Cellagentech), Bovine serum albumin (5 μg/ml, Sigma), hLIF (10 ng/ml, Millipore), Compound E (0.1 μM, EMD Millipore), Glutamax (Invitrogen), Pen/Strep, supplemented with N2 and B27 (Invitrogen), was added to the culture. After 6 days of differentiation, pNPCs were dissociated with Accutase (Invitrogen) and plated, with the aid of ROCK inhibitor (Y-27632, 3 μM, Cellagentech), onto culture dishes pre-coated with Matrigel (2%, BD Biosciences).

Neural rosette formation assays were performed using two independent protocols. The mono-layer method was adapted from a previously published protocol (Shi et al., 2012). iPSCs were passaged onto dishes pre-coated with Matrigel at about 50% confluence. The next day, medium containing DMEM:F12, non-essential amino acids, 2-Mercaptoethanol, Glutamax, Dorsomorphin (1 μM, Sigma), SB431542 (3 μg/ml), retinoic acid (1 μM), supplemented with N2 and B27, was added and cells were cultured for 10-17 days or until neural rosette formation. For neural rosette formation using embryoid bodies (Juopperi et al., 2012), iPSCs were detached with Collagenase Type IV and cultured on ultra-low attachment dishes for 4 days in standard human embryonic stem cell medium, which was switched to neurosphere medium, containing Neurobasal medium with B27, glutamax and 10 ng/ml bFGF, for the next 10 days. Embryoid bodies were transferred to dishes pre-coated with Matrigel and culture in neurosphere medium for 5-7 days or until neural rosette formation. Neural rosettes were fixed and immunostained with antibodies for atypical PKCλ, N-cadherin, PAR3 or β-catenin. Neural rosettes were initially identified based on polarized pattern of DAPI staining and NESTIN immunoreactivity. Only

individual non-overlapped neural rosettes that were 50-200 μm in diameter were included for quantification. The number of rosettes showing an intact apical-ring structure (more than 90% of coverage of apical-ring circumference with atypical PKCλ, N-cadherin, PAR3 or β-catenin immunoreactivity) and incomplete/partial apical structure (less than 90% coverage) were quantified. The quantifications were performed with at least three independent cultures.

DNA Constructs and Quantitative PCR

For mouse studies, short hairpin RNA sequences (Table S3) were cloned into the retroviral vector expressing GFP under the control of the EF1α promoter and the specific shRNA under the control of human U6 promoter (pUEG) as previously described (Duan et al., 2007). For the knockdown of human *CYFIP1* in pNPCs, short hairpin sequences against human *CYFIP1* were cloned into the lentiviral vector expressing GFP under the control of the human ubiquitin C promoter and the specific shRNA under the control of human U6 promoter (cFUGW: Addgene plasmid 14883). Previously characterized shRNAs against mouse *Cyfip1* (Silva et al., 2009), mouse *Abi1* (Sun et al., 2008), mouse *Arp2* (Wu et al., 2012) and human *CYFIP1* (Silva et al., 2009) were used and the efficacy of each shRNA was confirmed in mouse or human NPCs. For rescue experiments in utero, full-length mouse CYFIP1 cDNA (Open Biosystems, Accesion: 5345535) was cloned into pCAGGS-IRES-eGFP with the addition of an N-terminal HA epitope tag, which is resistant to the 3'UTR targeting shRNA-*Cyfip1*#2. For the production of CYFIP1-overexpressing iPSC lines, full-length CYFIP1 cDNA was cloned into a lentiviral vector (Suter et al., 2006) by gateway cloning.

For gene expression analysis, total RNA fraction was immediately isolated from cultured pNPC samples with RNeasy Mini Kit (Qiagen), treated with DNaseI and reverse-transcribed into the first-strand cDNA with SuperScript III (Invitrogen). cDNAs were used for SYBR-green based quantitative real-time PCR to measure the expression level of target genes with the ΔΔT method (ABI). The following primers were used for quantitative PCR: human CYFIP1 (forward: 5'-ATGCATGTGGACGAGTGTGT-3'; reverse: 5'-GATCATACAGCCAGCCCAGT-3'); human WAVE2 (forward: 5'-TCTGATACCACCAAGCCCAA-3'; reverse: 5'-CACAACATCCCGCTTCTCTT-3'); human GAPDH (forward: 5'-TGATGACATCAAGAAGGTGGTGAAG-3'; reverse: 5'-TCCTTGGAGGCCATGTGGGCCAT-3').

Cell Culture and Transfection/infection

HEK293-GP cells were cultured in DMEM containing 10% FBS (Hyclone, Logan, UT, USA), 4 mM L-glutamine (Gibco BRL), 100 IU/ml penicillin (Gibco BRL) and 100 μg/ml streptomycin (Gibco BRL). Mouse neural progenitors were cultured in Neurobasal medium (Gibco BRL) containing 20 ng/ml FGF2, 20 ng/ml EGF, 5 mg/ml heparin, 2% B27 (v/v, Gibco BRL), 4 mM L-glutamine as previously described (Kim et al., 2009). High titer retrovirus and lentivirus were produced from HEK293-GP cells and used to infect mouse or human NPCs in the presence of 4 μg/ml polybrene (Milipore) as previously described (Kim et al., 2009).

Co-immunoprecipitation and Western Blot Analysis

For co-IP analysis, forebrain tissues or NPCs were homogenized in the lysis buffer [10 mM Tris (pH 7.5), 150 mM NaCl, 5 mM EDTA, 1% Triton-X 100, 1 mM Na_3VO_4, 1 mM NaF, 1 mM DTT] containing protease inhibitor cocktails (Sigma-Aldrich). The lysates were incubated for 15 min on ice and centrifuged for 15 min at 15,000 × g 4°C. The supernatant was collected as cytosolic protein extract. Samples were immunoprecipitated with 20 μg of anti-CYFIP1 antibodies (Milipore), and then subjected to Western blot analysis. For Western blotting, 25-40 μg of supernatants or immunoprecipitants were separated by 10% SDS-PAGE, transferred to nitrocellulose membranes (BioRad), incubated with primary and secondary antibodies and visualized with SuperSignal West Dura Chemiluminescent Substrate (Thermo Scientific). Primary antibodies are listed in Table S2. Quantification of bands was performed using ImageJ software.

In utero Electroporation and Quantitative Analysis of Mouse Cortical Development

In utero electroporation was performed as described (Saito, 2006). In brief, timed-pregnant CD1 mice (Charles River) at E13.5 were anesthetized, uterine horns were exposed and

approximately 1 to 2 µl of plasmid DNA (1 µg/µl) was injected manually into lateral ventricles of embryos using a beveled and calibrated micropipette. Five pulses (40 V, 50 ms in duration with a 950 ms interval) were delivered across each uterus with two 5 mm-electrode paddles positioned on either side of the head (CUY650-5, Nepa Gene) by a CUY21SC electroporator (Nepa Gene). After electroporation, the uterus was placed back in the abdominal cavity and the wound was sutured. For EdU labeling, mouse embryos were electroporated at E13.5 and EdU (150 mg/kg bodyweight, Invitrogen) was injected at 2 or 24 hours before analysis.

For quantitative analysis of electroporated neocortices, GFP^+ cells localized within the dorso-lateral cortex were examined. A total of 3–6 brain sections were analyzed per animal by taking 3x3 images to cover the electroporated region of each coronal section with a 25× or 40× objective and comparing them with equivalent sections in littermate counterparts. Quantifications were performed using Imaris software (Bitplane). For distribution plots, the distances between GFP^+Pax6^+ cells or GFP^+Tbr2^+ cells and the ventricular surface were calculated by using an in-house MATLAB script (The MathWorks, Inc.), and plotted after dividing each distance by total length of the neocortex and subgrouping into ten equal-size vertical bins (1: the most apical, 10: the most basal).

All animal procedures were performed in accordance with the protocol approved by the Institutional Animal Care and Use Committee.

Immunohistochemistry and Immunocytochemistry

For immunostaining of tissue sections and whole-mount brains, brains of embryos were fixed with 4% paraformaldehyde (PFA) in PBS overnight at 4°C. Brains were cryoprotected in 30% sucrose in PBS, embedding in OCT compound, and sectioned coronally (20 µm-thickness) on a Leica CM3050S cryostat. For immunostaining of cultured iPSCs or neural rosettes, cells were fixed with 4% PFA in PBS for 20 min at 4°C. Brain sections and cells were blocked and permeabilized with 5% normal donkey serum (NDS), 3% Bovine serum albumin (BSA) and 0.1% Triton X-100 in PBS for 1 hr at room temperature, followed by incubation with primary antibodies diluted in 5% NDS, 3% BSA and 0.1% Triton X-100 in PBS at 4°C overnight. Primary antibodies and concentrations for experiments are listed in Table S2. Fluorescent secondary antibodies were used according to the manufacturer's protocol (Jackson ImmunoResearch). Nuclei were visualized by incubating for 10 min with 0.1 mg/ml 4,6-diamidino-2-phenylindole (DAPI; Sigma-Aldrich) in PBS. F-actin filaments were labeled by incubation in Alexa 594-labeled phalloidin (Invitrogen). For en face view of the ventricular surface, whole-mount stained neocortices were microdissected into small pieces (1 mm x 1 mm) and mounted on glass slides. Stained sections were mounted with ProLong Gold antifade reagents (Invitrogen) and analyzed using confocal scanning microscopes (Zeiss LSM 710).

mRNA Expression Analysis of Post-mortem Human Brains

mRNA expression data were generated from post-mortem DLPFC grey matter from 64 subjects without history or diagnosis of a medical or psychiatric disorder (51 males; mean age: 44 ± 14.9 years), all from European ancestry population and matched on age and various post-mortem tissue characteristics. Detailed methods relating to the Brain Tissue Collection of the Clinical Brain Disorders Branch at NIMH (CBDB/NIMH) and the Lieber Institute for Brain Development (LIBD) have been described elsewhere (Colantuoni et al., 2011). In brief, post-mortem human brains from the Brain Tissue Collection of CBDB/NIMH and LIBD were obtained at autopsy. Clinical characterization, diagnoses, and macro- and microscopic neuropathological examinations, toxicological analysis, RNA extraction, and quality control measures were performed using a standardized paradigm as previously described (Colantuoni et al 2011). Subjects with evidence of neuropathology, or drug or alcohol abuse, were excluded from analyses. Processing of post-mortem PFC grey matter tissue homogenates was as follows: Poly-A containing mRNA molecules were purified from 1 µg DNAse treated total RNA. Following purification, the mRNA was fragmented into small pieces using divalent cations under elevated temperature. Reverse transcriptase and random primers were used to copy the cleaved RNA fragments into first strand cDNA. The second strand cDNA was synthesized using DNA Polymerase I and RNaseH. These cDNA fragments then went through an end repair process using T4 DNA polymerase, T4 PNK and Klenow DNA polymerase, and the addition of a single

'A' base using Klenow exo (3' to 5' exo minus), then ligation of the Illumina PE adapters using T4 DNA Ligase. An index (up to 12) was inserted into Illumina adapters so that multiple samples could be sequenced in one lane of an 8-lane flow cell if necessary. These products were then purified and enriched with PCR to create the final cDNA library for high-throughput DNA sequencing using the Illumina Highseq 2000. The Illumina Real Time Analysis (RTA) module was used to perform image analysis and base calling, followed by use of BCL Converter (CASAVA v1.8.2) to generate FASTQ files containing sequence reads. 100 bp paired-end reads of cDNA sequences obtained by the Highseq2000 were aligned back to the human genome reference (UCSC hg19) by splice-read mapper (TopHat v2.0.4), providing known transcripts from Ensembl Build GRCh37.67 (Trapnell et al., 2009). To quantify gene-level expression, we used htseq-count v0.5.3 (with intersection-strict mode) to count the properly-paired and mapped reads and RPKM (Reads Per Kilobase per Million mapped reads) was calculated (Anders, 2010). Average read depth is 80-100 fold coverage.

SNP Genotyping and Gene Expression Analysis

DNA for genotyping was obtained from the cerebella of samples in the collection using Illumina OMNI 2.5M SNP chips. Genotypes were called using BeadExpress software. Quality control (QC) was performed after genotype-calling from the intensity plots using the Illumina GenomeStudio (Illumina, version 2010.1). SNPs with minor allele frequencies < 1%, high missing rates (> 5%) and deviation from Hardy-Weinberg expectation ($p < 0.0001$) were removed. Individuals also were removed from analysis if their genotyping rate was below 97%. The cis-association analysis of genetic variants within each gene was assessed using analysis of covariance to identify specific potential functional SNPs for gene-gene interaction analysis. SNPs associated with gene expression were included in the interaction analyses. We also included in the interaction analysis SNP rs4778334, recently reported as associated with schizophrenia in a Han Chinese sample (Zhao et al., 2013) and also associated with *CYFIP1* expression in our post-mortem samples ($p = 0.05$). We used ANCOVAs, with age, sex and RIN (RNA Integrity Number) as covariates, to investigate main effects of SNPs on gene expression.

Clinical Genetic Association and Interaction Analyses

We carried out clinical genetic association and interaction analyses using logistic regression in four independent sample cohorts of cases with schizophrenia and healthy controls. Final interaction analysis was also assessed in the combined sample of four cohorts while controlling cohort effect in order to gain adequate power to detect interactions. The sample collection, genotyping and quality control have been described elsewhere (Zhang et al., 2011). In brief, the four sample cohorts were the following: a first sample from LIBD/CBDB with addition of normal controls from published datasets that were used for a genome-wide association study of alcohol dependence (Zuo et al., 2012) and shared normal controls of Americans acquired from the iControlDB of Illumina Company (http://www.illumina.com/ science/ icontroldb.ilmn) (total sample, 413 cases and 2,432 controls); all these samples were genotyped using Illumina HumanHap 550K/1M platforms and went through heterogeneity reduction by removing multivariate outliers through identity by state and multidimensional scaling analysis. The second cohort, including 2126 subjects (936 cases and 1190 controls), was from Caucasian Americans and obtained from first release of genetic association information network (GAIN) genotyped using Affymetrix 6.0; the third and the fourth cohorts were from Scotland (n = 1137; 537 cases and 540 controls) and Germany (n = 1033; 518 cases and 517 controls), respectively; these samples were genotyped using the Illumina 330K platforms.

References

Anders, S. (2010). HTSeq: Analysing high-throughput sequencing data with Python (Heidelberg, Germany, European Molecular Biology Laboratory, Genome Biology Unit).

Chiang, C. H., Su, Y., Wen, Z., Yoritomo, N., Ross, C. A., Margolis, R. L., Song, H., and Ming, G. L. (2011). Integration-free induced pluripotent stem cells derived from schizophrenia patients with a DISC1 mutation. Mol Psychiatry *16*, 358-360.

Juopperi, T. A., Kim, W. R., Chiang, C. H., Yu, H., Margolis, R. L., Ross, C. A., Ming, G. L., and Song, H. (2012). Astrocytes generated from patient induced pluripotent stem cells recapitulate features of Huntington's disease patient cells. Mol Brain *5*, 17.

Kim, J. Y., Duan, X., Liu, C. Y., Jang, M. H., Guo, J. U., Pow-anpongkul, N., Kang, E., Song, H., and Ming, G. L. (2009). DISC1 regulates new neuron development in the adult brain via modulation of AKT-mTOR signaling through KIAA1212. Neuron *63*, 761-773.

Li, W., Sun, W., Zhang, Y., Wei, W., Ambasudhan, R., Xia, P., Talantova, M., Lin, T., Kim, J., Wang, X.*, et al.* (2011). Rapid induction and long-term self-renewal of primitive neural precursors from human embryonic stem cells by small molecule inhibitors. Proc Natl Acad Sci U S A *108*, 8299-8304.

Mattai, A. A., Weisinger, B., Greenstein, D., Stidd, R., Clasen, L., Miller, R., Tossell, J. W., Rapoport, J. L., and Gogtay, N. (2011). Normalization of cortical gray matter deficits in nonpsychotic siblings of patients with childhood-onset schizophrenia. J Am Acad Child Adolesc Psychiatry *50*, 697-704.

Nguyen, H. N., and Reijo Pera, R. A. (2008). Metaphase Spreads and Spectral Karyotyping of Human Embryonic Stem Cells. CSH Protocols *doi:10.1101/pdb.prot5047*.

Silva, J. M., Ezhkova, E., Silva, J., Heart, S., Castillo, M., Campos, Y., Castro, V., Bonilla, F., Cordon-Cardo, C., Muthuswamy, S. K.*, et al.* (2009). Cyfip1 is a putative invasion suppressor in epithelial cancers. Cell *137*, 1047-1061.

Sun, X., Li, Y., Yu, W., Wang, B., Tao, Y., and Dai, Z. (2008). MT1-MMP as a downstream target of BCR-ABL/ABL interactor 1 signaling: polarized distribution and involvement in BCR-ABL-stimulated leukemic cell migration. Leukemia *22*, 1053-1056.

Trapnell, C., Pachter, L., and Salzberg, S. L. (2009). TopHat: discovering splice junctions with RNA-Seq. Bioinformatics *25*, 1105-1111.

Wu, C., Asokan, S. B., Berginski, M. E., Haynes, E. M., Sharpless, N. E., Griffith, J. D., Gomez, S. M., and Bear, J. E. (2012). Arp2/3 is critical for lamellipodia and response to extracellular matrix cues but is dispensable for chemotaxis. Cell *148*, 973-987.

Zhao, Q., Li, T., Zhao, X., Huang, K., Wang, T., Li, Z., Ji, J., Zeng, Z., Zhang, Z., Li, K.*, et al.* (2013). Rare CNVs and tag SNPs at 15q11.2 are associated with schizophrenia in the Han Chinese population. Schizophr Bull *39*, 712-719.